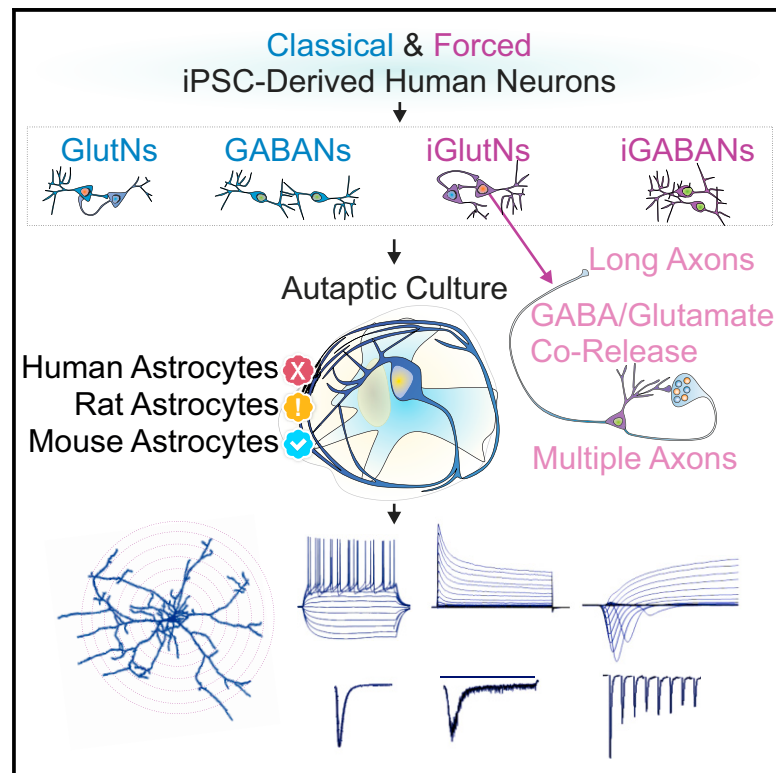


Cell Reports

An Autaptic Culture System for Standardized Analyses of iPSC-Derived Human Neurons

Graphical Abstract



Authors

Hong Jun Rhee, Ali H. Shaib, Kristina Rehbach, ..., Nils Brose, Oliver Brüstle, Jeong Seop Rhee

Correspondence

brustle@uni-bonn.de (O.B.),
rhee@em.mpg.de (J.S.R.)

In Brief

Rhee et al. establish an autaptic culture system of single iPSC-derived human neurons on astrocyte micro-islands, which allows for standardized assays of neuronal morphology, membrane properties, synapse function, and synaptic short-term plasticity.

Highlights

- Quality of human autapses depends on astrocyte type and fetal bovine serum additives
- Standardized assays of key morphological, biophysical, and synaptic properties
- Standardized assays of short-term plasticity, synaptic depression, and synapse recovery
- Some NGN2-induced neurons show multiple/long axons and glutamate-GABA corelease



An Autaptic Culture System for Standardized Analyses of iPSC-Derived Human Neurons

Hong Jun Rhee,^{1,6} Ali H. Shaib,^{1,6} Kristina Rehbach,^{2,3,6} ChoongKu Lee,¹ Peter Seif,^{1,4} Carolina Thomas,¹ Erinn Gideons,¹ Anja Guenther,¹ Tamara Krutenko,² Matthias Hebisch,² Michael Peitz,^{2,5} Nils Brose,¹ Oliver Brüstle,^{2,*} and Jeong Seop Rhee^{1,7,*}

¹Max Planck Institute of Experimental Medicine, Department of Molecular Neurobiology, Göttingen, Germany

²Institute of Reconstructive Neurobiology, University of Bonn School of Medicine & University Hospital Bonn, Bonn, Germany

³LIFE & BRAIN GmbH, Cellomics Unit, 53127 Bonn, Germany

⁴German University in Cairo, Cairo, Egypt

⁵Cell Programming Core Facility, University of Bonn School of Medicine, Bonn, Germany

⁶These authors contributed equally

⁷Lead Contact

*Correspondence: brustle@uni-bonn.de (O.B.), rhee@em.mpg.de (J.S.R.)

<https://doi.org/10.1016/j.celrep.2019.04.059>

SUMMARY

iPSC-derived human neurons are expected to revolutionize studies on brain diseases, but their functional heterogeneity still poses a problem. Key sources of heterogeneity are the different cell culture systems used. We show that an optimized autaptic culture system, with single neurons on astrocyte feeder islands, is well suited to culture, and we analyze human iPSC-derived neurons in a standardized, systematic, and reproducible manner. Using classically differentiated and transcription factor-induced human glutamatergic and GABAergic neurons, we demonstrate that key features of neuronal morphology and function, including dendrite structure, synapse number, membrane properties, synaptic transmission, and short-term plasticity, can be assessed with substantial throughput and reproducibility. We propose our optimized autaptic culture system as a tool to study functional features of human neurons, particularly in the context of disease phenotypes and experimental therapy.

INTRODUCTION

Modern methods to generate human induced pluripotent stem cells (iPSCs) and to differentiate them by cell type are expected to transform investigations of the molecular and cellular basis of neurological and psychiatric brain diseases (Blanpain et al., 2012; Hanna et al., 2010; Okita and Yamanaka, 2011; Takahashi and Yamanaka, 2016; Yang et al., 2017). Information on genetic disease causes is accumulating, but native patient tissue can rarely be obtained, genetically modified animal models of polygenic diseases cannot be generated, and animal disease models can have limited predictive validity (Jucker, 2010). Accordingly, many studies examined human neurons derived from embryonic stem cells (ESCs) or from iPSCs of healthy donors and patients.

Despite this progress, individual iPSC lines can differ substantially, leading to corresponding differences in derived neurons (Osafune et al., 2008; Takahashi and Yamanaka, 2016; Yang et al., 2017). Neurons derived by the same protocol from the same ESC or iPSC line can have different properties (Volpato et al., 2018; Wu et al., 2007), and mass cultured neurons derived from stem cells have massively diverse maturation states (Bardy et al., 2016; Dolmetsch and Geschwind, 2011). The causes of these discrepancies are manifold and include not only the induction protocol and cell line used but also the culturing method, medium composition, starting cell number, and co-cultured astrocytes (Bardy et al., 2016; Johnson et al., 2007; Shi et al., 2012a; Tang et al., 2013; Weick et al., 2010). These sources of heterogeneity in human ESC or iPSC-derived neurons represent a severe limitation to the analysis of—often subtle—disease-related neuronal phenotypes.

To circumvent these problems, we developed an autaptic culture system for iPSC-derived human neurons. This culture system, with single neurons on astrocyte micro-islands, is ideally suited for standardized and systematic analyses of morphological, biophysical, and functional features of neurons and their synapses (Burgalossi et al., 2012), particularly knockout phenotypes (Wojcik and Brose, 2007) and disease-related protein mutations (Lipstein et al., 2017). We optimized medium conditions and astrocyte micro-islands to provide a well-controlled autaptic culture protocol that generates morphologically mature and functionally active human iPSC-derived glutamatergic and γ -aminobutyric acid-ergic (GABAergic) neurons, in which key morphological, biophysical, and synaptic properties can be assessed reproducibly as they develop *in vitro*.

RESULTS

Generation of Human Neurons

Human iPSC-derived glutamatergic neurons (GlutNs) and GABAergic forebrain neurons (GABANs) were generated by either small-molecule and morphogen treatment (classical differentiation) or transcription factor-based forward programming to generate induced GABAergic neurons (iGABANs) and induced



glutamatergic neurons (iGlutNs). The forward programming of iGlutNs is described in the accompanying paper in this issue of *Cell Reports* (Meijer et al., 2019).

To generate GlutNs, a published protocol (Shi et al., 2012b) was optimized to achieve a high degree of purity and reproducibility by defining cell numbers and inhibiting growth factor pathways with the MEK/ERK inhibitor PD0325901 and the γ -secretase/Notch-signaling inhibitor DAPT (Dovey et al., 2001), yielding an almost pure neuronal population after 50 days of differentiation (Figure S1A). GABANs were generated by culturing iPSCs in E8 medium and increasing concentrations of the dual SMAD inhibitors SB431542 and LDN-193189 to obtain a highly enriched population of neurons with mostly GABAergic phenotype by 4 weeks of differentiation (Figure S1B).

To shorten maturation times, a forward programming strategy with forced DLX2 and ASCL1 expression was employed to generate iGABANs (Yang et al., 2017). To achieve homogeneous transgene expression, genome editing was used to target a third-generation (3G) tetracycline-inducible system (Qian et al., 2014) carrying human DLX2 and ASCL1 into both safe-harbor AAVS1 alleles. Avoiding random insertion and position-dependent effects on transgene expression, this approach yields iPSC clones that can be expanded to produce large batches of neurons, further reducing variability. Conversion into postmitotic iGABANs was promoted by DAPT and Ara-C, resulting in almost pure neuronal populations after only 9 days of transgene induction (Figure S1E). The same approach was used to obtain iGlutNs via forced expression of NGN2 (Meijer et al., 2019).

Derived neurons were cryopreserved as aliquots and validated before downstream analyses. Post-thaw viability was >80% (GlutNs, 86%; GABANs, 95%; and iGABANs, 85%) (Figure S1F). Based on immunofluorescence analysis, GlutNs were largely positive for β 3-tubulin (99%); 96.1% expressed the forebrain marker FOXG1, 90% expressed the Glut marker VGlut1, and only 2% contained GABA. GlutNs mainly expressed the layer VI- and layer V-specific markers TBR1 (81%) and CTIP2 (67%), respectively. Markers of upper cortical layers were only found in a subset of cells (BRN2, 11%, and SATB2, 3%), indicating that this protocol yields a Glut cortical population highly enriched for deep-layer neurons (Figures S1D and S1G). GABANs were 99.8% β 3-tubulin positive, and most of them were positive for the neurotransmitter GABA (87%) with only occasional cells (1%) expressing the Glut marker VGlut2; 96% of cells were positive for the forebrain marker FOXG1, whereas only 1% expressed the cortical marker TBR1 (Figure S1E and S1H). About 97% of iGABANs expressed the neuronal marker β 3-tubulin, 94% expressed the forebrain marker FOXG1, and only 0.4% expressed the Glut marker VGlut2; 89% contained the neurotransmitter GABA (Figures S1E and S1I). Most iGABANs were positive for parvalbumin; additional markers detected include calbindin, calretinin, and somatostatin (Figure S1J).

iPSCs and cryopreserved neurons were subjected to quality control (QC), including SNP-based copy number variation (CNV) analysis combined with gene ontology term filter for brain development and synapse genes to ensure genomic integrity (Meijer et al., 2019). Altogether, highly enriched cryopreservable neurons were generated, which enable the generation of standardized, long-term cultures without the risk of overgrowing re-

sidual neural precursors, making them suitable for comparative analyses at different sites.

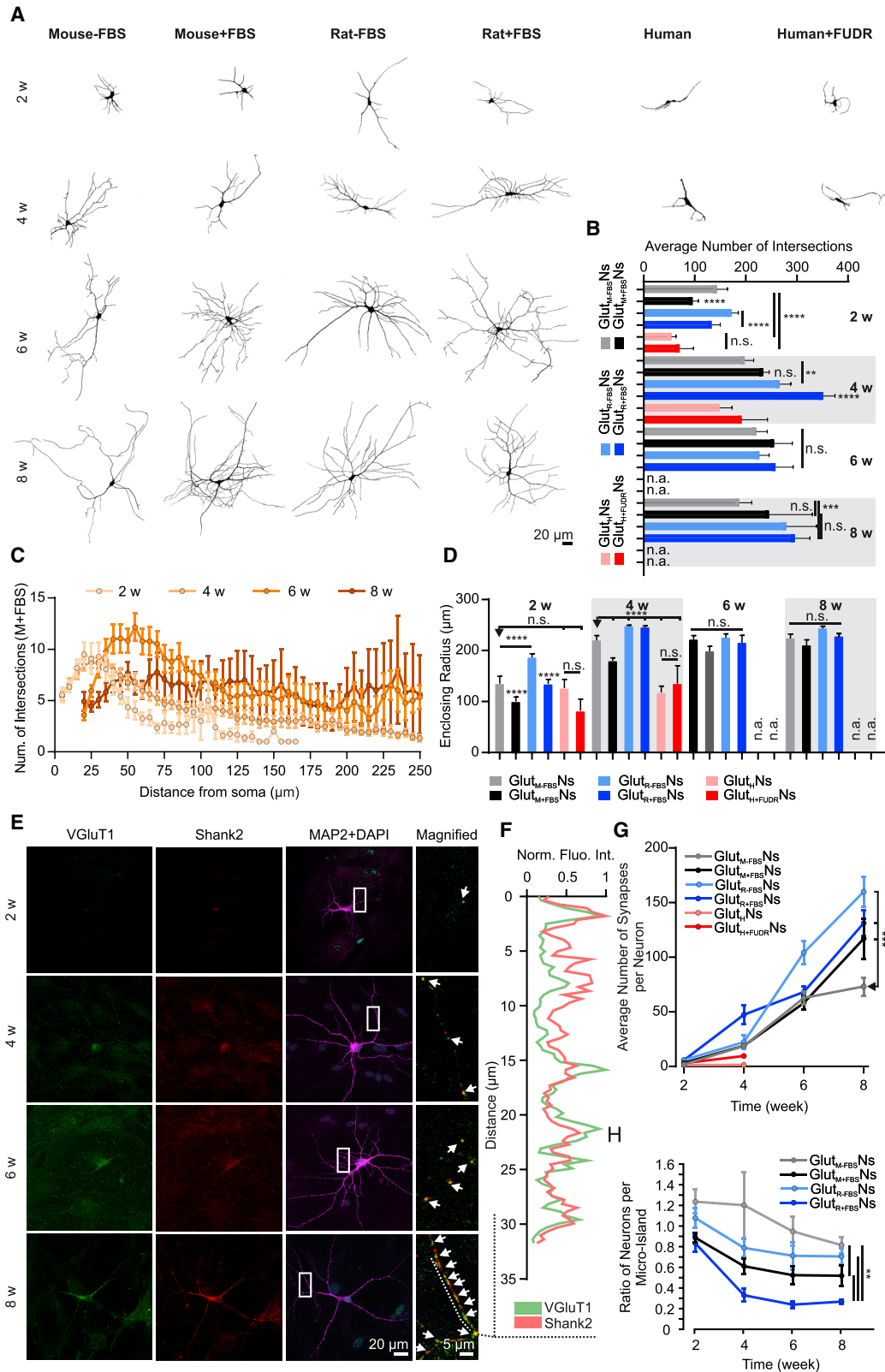
All experiments were based on GlutNs, GABANs, iGlutNs, iGABANs, and mouse cortical neurons for comparison (Table S1).

Human Cortical Glut Neurons Thrive in Autaptic Culture

Because human iPSC-derived neurons mature more slowly *in vitro* than rodent neurons, we tested the ability of rat and mouse astrocytes and of a human astrocyte cell line to support long-term autaptic cultures of GlutNs (Figure S1). We did not use purchasable human primary astrocytes, because (1) our intention was to develop an inexpensive routine method and (2) at least with mouse and rat primary astrocytes, freshly prepared, unpassaged cells are needed for micro-island cultures (Burgalossi et al., 2012). We tested the optimal fetal bovine serum (FBS) concentration (range 0.25%–10%) in N3 medium to maintain astrocytes in long-term culture and found that concentrations above or below 0.5% led to cell loss. We then assessed the optimal seeding number of human neurons (range 0.5×10^3 to 100×10^3 per 100 mm² micro-island astrocyte coverslip) (Burgalossi et al., 2012) and found 3,500–8,000 cells per 100 mm² micro-island astrocyte coverslip to be optimal.

We next tested rat, mouse, and human astrocytes more systematically using N3 medium (Shi et al., 2012a, 2012b) or N3 medium with 0.5% FBS (the osmolarity of the different culturing conditions was screened) (Figures S1K and S1L). Cells were fixed after 2, 4, 6, and 8 weeks *in vitro* and labeled for the dendrite and soma marker MAP2, the presynaptic marker VGlut1, and the postsynaptic marker Shank2. To assess neuronal growth, we assayed dendrite complexity by Sholl analysis (Deshpande et al., 2017; Sholl, 1953). Differences between astrocyte types and culture conditions were apparent at 8 weeks (Figure 1A). GlutNs co-cultured with mouse astrocytes without/with FBS (Glut_{M-FBS}Ns/Glut_{M+FBS}Ns) and rat astrocytes without/with FBS (Glut_{R-FBS}Ns/Glut_{R+FBS}Ns) developed better in culture (average dendritic intersections of 143.1 ± 20.7 , 95.9 ± 11.4 , 171.6 ± 13.6 , and 132.8 ± 17.4 , respectively) than neurons on human astrocytes without/with 20 μ M floxuridine (H/H+FUDR, added to prevent further astrocyte division) (54.3 ± 9.1 and 70.3 ± 27.3 intersections, respectively) (Figure 1B). At 2 weeks, cultured neurons in the presence of FBS showed less complex dendrites, but this changed around 4 weeks, when neurons in FBS improved (e.g., Glut_{R+FBS}Ns, 350.6 ± 24.0 intersections, and Glut_{R-FBS}Ns, 265.8 ± 21.9 intersections) (Figure 1B). All conditions allowed neurons to thrive, except when human astrocytes were used; these did not support neuron survival beyond 4 weeks (Figures 1A–1D).

To assess synaptogenesis, we counted colocalizing puncta of immunolabeled VGlut1 and Shank2 (Figures 1E and 1F). GlutNs cultured with human astrocytes hardly formed any synapses, while Glut_{R-FBS}Ns and Glut_{R+FBS}Ns developed the highest numbers of synapses (160.0 ± 13.7 and 131.2 ± 12.9 , respectively) (Figure 1G). In comparison, Glut_{M-FBS}Ns and Glut_{M+FBS}Ns developed significantly fewer synapses (73.2 ± 8.1 and 117.0 ± 18.2 , respectively) (Figure 1G). In parallel, we quantified neuronal survival, expressed as the ratio of neurons per micro-island (Figure 1H). At 2 weeks, ratios of 1.3 ± 0.1 , 0.9 ± 0.04 , 1.1 ± 0.1 ,



(legend on next page)

and 0.8 ± 0.1 were observed for the M–FBS, M+FBS, R–FBS, and R+FBS conditions, respectively. Ratios decreased over time under all conditions, most prominently with R+FBS cells, whose ratio was only 0.26 ± 0.02 at 8 weeks, while the M–FBS condition had the highest survival rate after 8 weeks (0.8 ± 0.1). These data show that cultured human GlutNs are viable for at least 8 weeks with mouse and rat astrocytes, with mouse astrocytes being superior in terms of neuronal survival (Figure 1H).

We assessed the maturation of Glut_{M+FBS}Ns by labeling MAP2 and doublecortin (DCX), a marker for immature neurons (Figures S2A and S2B). DCX levels dropped significantly after 2 weeks, while MAP2 levels increased (Figures S2C–S2E). DCX levels remained constant in neurite tips (Figures S2F and S2G), reflecting ongoing growth (Spampanato et al., 2012).

Human Cortical GlutNs Show Proper Membrane Properties

Autaptic GlutNs showed evoked postsynaptic potential (PSP) and five action potential (AP) firing patterns upon depolarization (Johnson et al., 2007): abortive (no APs), phasic I (single AP), phasic II (multiple APs during the early phase of depolarization), tonic (APs throughout depolarization), and spontaneous (irregular APs even without depolarization) (Figure S3). Input resistances (R_{input}) of the different neuron groups were similar, except that phasic I neurons had a lower R_{input} (Figures S3Bi and S3Bii). At 8 weeks, 90% of Glut_{M+FBS}Ns exhibited a tonic firing pattern (Figures 2A and 2B), while 90% of Glut_{M–FBS}Ns showed a tonic firing pattern at 6 weeks (Figures 2C and 2D). Glut_{R–FBS}Ns and Glut_{R+FBS}Ns exhibited properties similar to those of cells cultured with mouse astrocytes (Figures S3F–S3I).

Resting membrane potentials (RMPs) of Glut_{M+FBS}Ns were -37.4 ± 2.5 mV at 2 weeks and decreased until 4 weeks to then stabilize (4 weeks, -51.6 ± 1.6 mV; 6 weeks, -55.5 ± 1.7 mV; and 8 weeks, -54.9 ± 1.5 mV), similar to autaptic mouse cortical neurons (-50.0 ± 1.5 mV) (Figures 2E and S6B). RMPs of Glut_{M–FBS}Ns were stable from 2 weeks onward (2 weeks, -44.5 ± 5.63 mV; 4 weeks, -51.5 ± 8.4 mV; 6 weeks, -46.4 ± 6.1 mV; and 8 weeks, -48.7 ± 4.9 mV) (Figure 2E). RMPs of Glut_{R+FBS}Ns and Glut_{R–FBS}Ns were similar to those of Glut_{M+FBS}Ns and Glut_{M–FBS}Ns (Figure S3J), indicating few RMP

differences between cells cultured on mouse or rat astrocytes. The capacitance, a measure of cell size, of Glut_{M+FBS}Ns and Glut_{M–FBS}Ns increased from 2 to 10 weeks (Figure 2F), as with Glut_{R+FBS}Ns and Glut_{R–FBS}Ns (Figure S3K). The R_{input} of Glut_{M+FBS}Ns and Glut_{M–FBS}Ns and of Glut_{R+FBS}Ns and Glut_{R–FBS}Ns decreased steadily and similarly over time (Figures 2G and S3L).

Active electrical properties of GlutNs were analyzed by recording threshold, overshoot, amplitude, and half-width of APs, and the afterhyperpolarization (AHP) amplitude. Overshoot and amplitude of APs in Glut_{M+FBS}Ns and Glut_{M–FBS}Ns increased from 2 to 8 weeks and then stabilized, while AP half-width decreased progressively and AHP amplitude remained stable (Figures 2H–2L). Similar data were obtained for Glut_{R+FBS}Ns and Glut_{R–FBS}Ns (Figures S3M–S3Q). Thus, active and passive electrical properties of GlutNs are not affected by FBS or astrocyte type.

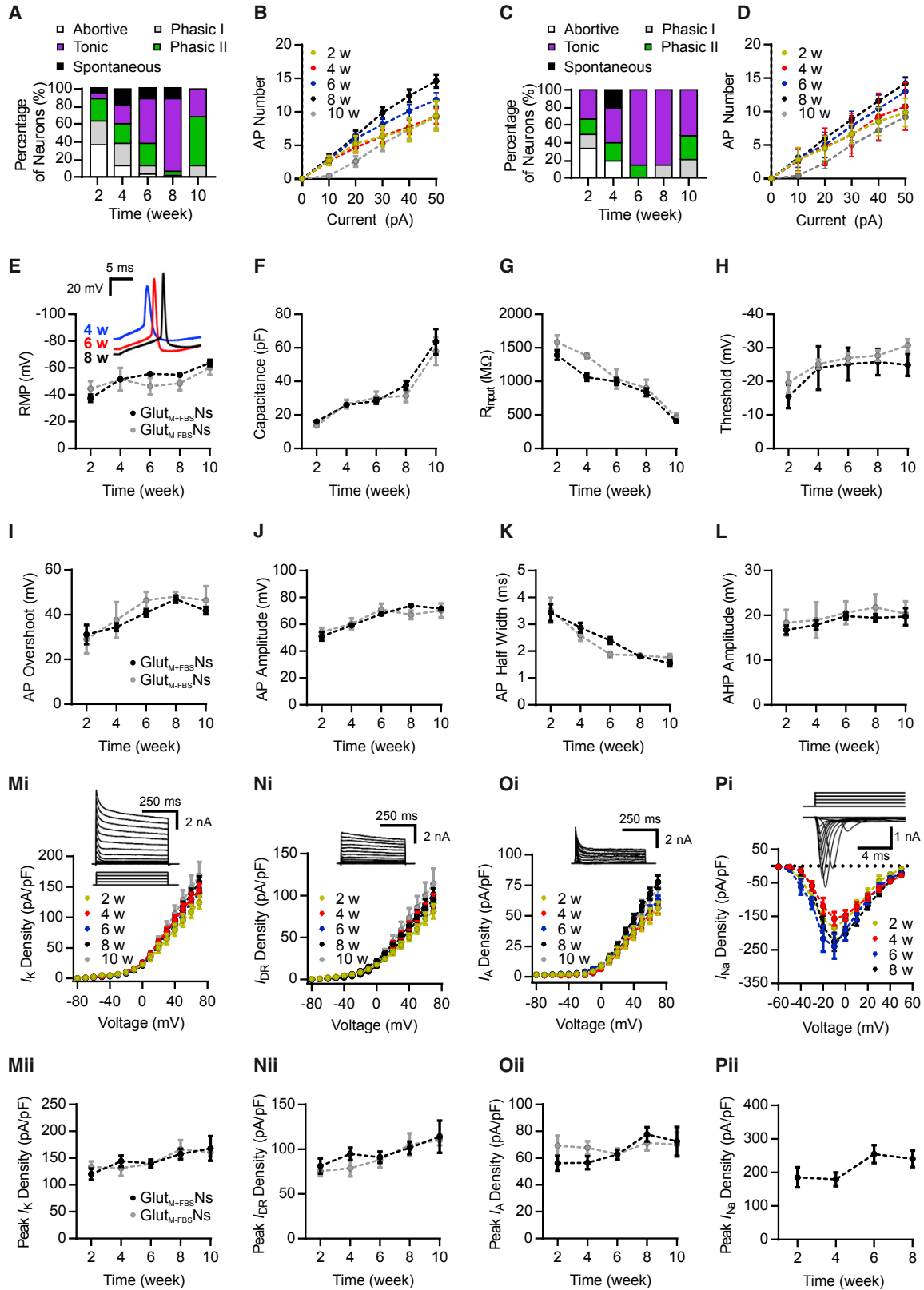
The density and activity of voltage-gated Na⁺ channels are the main determinants of AP overshoot and amplitude. The magnitudes of AP overshoot and amplitude increased with time in all tested cells (Figures 2I, 2J, S3N, and S3O), indicating that the density of voltage-gated sodium currents (I_{Na}) increased. I_{Na} of Glut_{M+FBS}Ns was evoked by 500 ms test pulses at 10 mV intervals between -80 and $+70$ mV from a holding potential of -70 mV, with or without 300 nM tetrodotoxin (TTX) (Figure S3D). The densities of peak I_{Na} in Glut_{M+FBS}Ns were not significantly different between 2 and 4 weeks (2 weeks, 185.8 ± 29.9 pA/pF, and 4 weeks, 179.5 ± 21.1 pA/pF) but larger at 6 weeks (255.0 ± 26.7 pA/pF) and 8 weeks (240.7 ± 25.3 pA/pF) (Figure 2P). The peak I_{Na} densities at 6 and 8 weeks in Glut_{M+FBS}Ns were similar to those of mouse cortical neurons (249.1 ± 41.6 pA/pF).

Voltage-gated K⁺ currents (I_K) determine width, repolarization, and frequency of APs. Voltage-clamp recordings were used to test whether delayed rectifier K⁺ currents (I_{DR}) and the transient A-type K⁺ currents (I_A) are correlated with AP maturation in Glut_{M+FBS}Ns and Glut_{M–FBS}Ns. Total K⁺ currents (I_K) were evoked by 500 ms depolarizing test pulses at $+10$ mV intervals between -80 and $+70$ mV from a holding potential of -70 mV; I_{DR} was recorded using the same protocol in the presence of 1 mM 4-aminopyridine (4AP). I_A traces were obtained by subtracting I_{DR} from I_K (Figure S3E). The density of I_A in Glut_{M+FBS}Ns

Figure 1. Morphological Analysis of Growth, Synapse Formation, and Survival of GlutNs

- (A) Representative binary images of GlutNs co-cultured with mouse and rat astrocytes in the presence or absence of FBS and with human astrocytes in the presence or absence of FUDR over the course of 8 weeks.
- (B) Average number of dendrites intersecting Sholl circles 5–250 μ m from the soma under the different culturing conditions (N = 2 independent experiments). M–FBS, M+FBS, R–FBS, R+FBS, H, and H⁺FUDR 2 weeks (n = 18, 18, 21, 21, 7, and 3) and 4 weeks (n = 14, 26, 21, 25, 7, and 7). M–FBS, M+FBS, R–FBS, and R+FBS, respectively, at 6 weeks (n = 20, 19, 20, and 19) and 8 weeks (n = 10, 13, 5, and 22). R, rat; M, mouse; H, human astrocytes.
- (C) Number of dendritic intersections of Glut_{M+FBS}Ns plotted as a function of distance from the soma over the course of 8 weeks.
- (D) Enclosing radius of dendrites measured from the soma (N = 2 independent experiments, as in B).
- (E) Representative confocal images of Glut_{M+FBS}Ns stained against presynaptic marker VGluT1, postsynaptic marker Shank2, and neuronal soma/dendrite marker MAP2, with DAPI staining, acquired at 2, 4, 6, and 8 weeks. White arrows point at synapses, and white rectangles indicate the position of the magnified regions of the images.
- (F) Sample line scan fluorescence intensity chart plotted as a function of distance measured over a neuronal process at 8 weeks.
- (G) Average number of synapses per neuron. M–FBS, M+FBS, R–FBS, R+FBS, H, and H⁺FUDR, respectively, at 2 weeks (n = 22, 22, 22, 24, 7, and 4) and 4 weeks (n = 34, 37, 22, 26, 7, and 7). M–FBS, M+FBS, R–FBS, and R+FBS, respectively, at 6 weeks (n = 34, 30, 28, and 26) and 8 weeks (n = 33, 34, 25, and 33).
- (H) Ratio of surviving neurons per micro-island. M–FBS, M+FBS, R–FBS, and R+FBS, respectively, at 2 weeks (n = 9, 7, 6, and 8), 4 weeks (n = 6, 8, 6, and 7), 6 weeks (n = 6, 5, 6, and 7), and 8 weeks (n = 7, 6, 8, and 7).

Data are displayed as mean \pm SEM. ANOVA on rank test was applied (*p < 0.05, **p < 0.01, ***p < 0.001, ****p < 0.0001; ns, not significant, p > 0.05).



(legend on next page)

and $\text{Glut}_{\text{M-FBS}}$ Ns increased between 2 weeks (124.2 ± 10.6 pA/pF) and 10 weeks (167.9 ± 23.2 pA/pF), as did the densities of I_{DR} and I_{A} (Figures 2M–2O). Instead, the density of I_{DR} and I_{A} in Glut_{R} Ns remained unchanged with time in culture (Figures S3R–S3T). AP maturation in Glut_{M} Ns and Glut_{R} Ns was similar at 8 weeks, but the densities of I_{DR} and I_{A} were lower in Glut_{R} Ns, indicating that mouse astrocytes support neuronal maturation slightly better than rat astrocytes.

Medium Composition and Astrocyte Origin Affect Synaptic Activity of Human Cortical GlutNs

Synaptic properties of $\text{Glut}_{\text{M+FBS}}$ Ns and $\text{Glut}_{\text{M-FBS}}$ Ns under different culturing conditions were studied using whole-cell voltage-clamp recordings. Evoked excitatory postsynaptic current (EPSC) amplitudes of $\text{Glut}_{\text{M+FBS}}$ Ns gradually increased until 10 weeks (2.66 ± 0.26 nA). Beyond 10 weeks, neurons were scarce, likely due to astrocyte death. $\text{Glut}_{\text{M-FBS}}$ Ns developed synaptic currents at 2 weeks, similar to $\text{Glut}_{\text{M+FBS}}$ Ns, but EPSC amplitudes then increased less prominently to only 0.82 ± 0.34 nA at 10 weeks (Figure 3A), indicating that FBS affects synapse number and function. Similar findings were obtained in assays of the readily releasable pool (RRP) of synaptic vesicles, as estimated by integrating charge transfer during hypertonic 0.5 M sucrose application for 6 s. While RRP sizes of $\text{Glut}_{\text{M+FBS}}$ Ns gradually increased over time, leveling off at 8 weeks (0.14 ± 0.01 nC), RRP sizes of $\text{Glut}_{\text{M-FBS}}$ Ns were smaller (Figure 3E). The vesicular release probabilities (P_{vr}), calculated by dividing the charge transfer of a single EPSC by the charge transfer of RRP release, were similar between $\text{Glut}_{\text{M+FBS}}$ Ns and $\text{Glut}_{\text{M-FBS}}$ Ns, although the P_{vr} of $\text{Glut}_{\text{M-FBS}}$ Ns fluctuated with time (Figure 3F). Thus, although the strength of synaptic transmission was higher in $\text{Glut}_{\text{M+FBS}}$ Ns than in $\text{Glut}_{\text{M-FBS}}$ Ns, the P_{vr} was similar. EPSC amplitudes, RRP, and P_{vr} in $\text{Glut}_{\text{R+FBS}}$ Ns and $\text{Glut}_{\text{R-FBS}}$ Ns cells were only measured between 7 and 10 weeks. During this period, the corresponding values did not change substantially, but they were consistently smaller in the absence of FBS (Figures 3C, 3G, and 3H).

We next recorded miniature EPSCs (mEPSCs) in 300 nM TTX. $\text{Glut}_{\text{M+FBS}}$ Ns had higher mEPSC amplitudes and frequencies

than $\text{Glut}_{\text{M-FBS}}$ Ns, which increased with time in culture (Figures 3I and 3J). mEPSC amplitudes and frequencies in $\text{Glut}_{\text{R+FBS}}$ Ns and $\text{Glut}_{\text{R-FBS}}$ Ns peaked at 8 weeks and were smaller in $\text{Glut}_{\text{R-FBS}}$ Ns at this time point (Figures 3K and 3L), again showing that FBS supports synaptic strength.

Diacylglycerol and phorbol esters stimulate transmitter release in rodent autapses via Munc13-family vesicle priming proteins and protein kinase C (PKC) (Rhee et al., 2002; Wierda et al., 2007). 3 μM phorbol 12,13-dibutyrate (PDBu) had a similar but less pronounced effect on $\text{Glut}_{\text{M+FBS}}$ Ns and $\text{Glut}_{\text{R+FBS}}$ Ns (Figures 3B and 3D), indicating that regulatory effects of Munc13s and PKC on transmitter release are similar in rodent and human neurons.

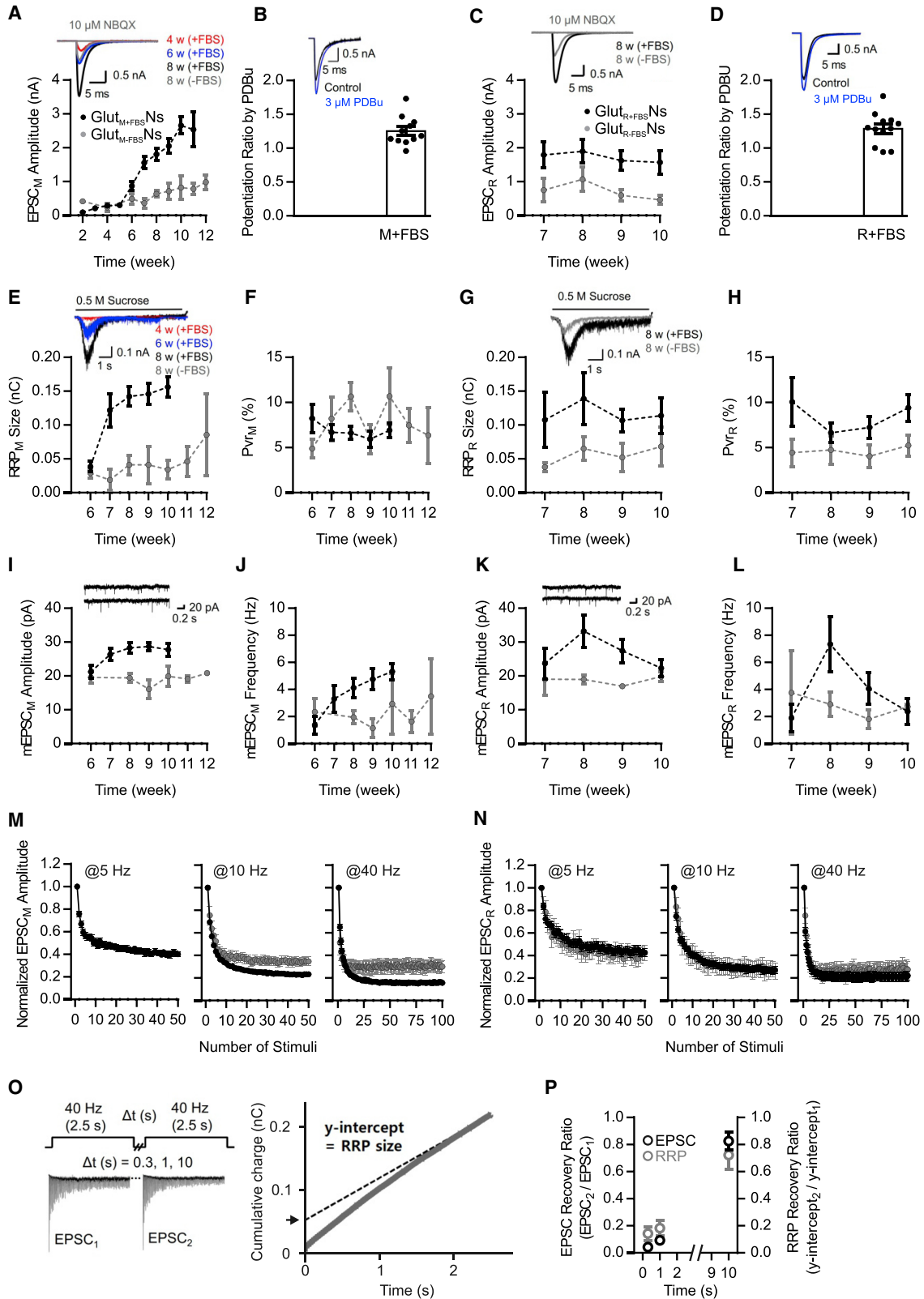
Autaptic cultures allow accurate analyses of synaptic short-term plasticity (STP), a key synaptic process (Regehr, 2012). Upon high-frequency stimulation (5, 10, and 40 Hz), $\text{Glut}_{\text{M+FBS}}$ Ns, $\text{Glut}_{\text{M-FBS}}$ Ns, $\text{Glut}_{\text{R+FBS}}$ Ns, and $\text{Glut}_{\text{R-FBS}}$ Ns showed strong synaptic short-term depression (STD) (Figures 3M and 3N), like mouse cortical neurons (Figure S6S), without an effect of the astrocyte type. Steady-state STD levels were slightly lower in $\text{Glut}_{\text{M+FBS}}$ Ns upon 10 and 40 Hz stimulation, but no such effect was seen in neurons cultured on rat astrocytes. By pairing 40 Hz stimulation trains at 0.3, 1, and 10 s intervals, we measured activity-dependent EPSC and RRP recovery in $\text{Glut}_{\text{M+FBS}}$ Ns. The recovery ratio was calculated by dividing the first EPSC amplitude of the second train by the first amplitude of the first train ($\text{EPSC}_2/\text{EPSC}_1$). RRP size was estimated by the back-extrapolation method (Neher, 2015). The RRP recovery ratio was calculated by dividing the estimated RRP size assessed during the second train by that of the first train ($\text{RRP}_2/\text{RRP}_1$). We did not detect differences in EPSC and RRP recovery ratios between $\text{Glut}_{\text{M+FBS}}$ Ns and mouse cortical neurons (Figures 3O, 3P, and S6T). Thus, key aspects of activity-dependent synaptic vesicle dynamics are similar in human and mouse cortical neurons.

Human Cortical GlutNs Thrive Best with Mouse Astrocytes and 0.5% FBS

Because $\text{Glut}_{\text{R+FBS}}$ Ns had lower survival rates than $\text{Glut}_{\text{M+FBS}}$ Ns, we investigated whether the different culture conditions stress

Figure 2. Electrophysiological Characterization of Glut_{M} Ns and Effects of Astrocyte Type and FBS

(A) AP firing types of $\text{Glut}_{\text{M+FBS}}$ Ns. At 8 weeks, most neurons were of the tonic AP firing type. $\text{Glut}_{\text{M+FBS}}$ Ns at 2 weeks (n = 19), 4 weeks (n = 59), 6 weeks (n = 75), 8 weeks (n = 57), and 10 weeks (n = 16); $\text{Glut}_{\text{M-FBS}}$ Ns at 2 weeks (n = 6), 4 weeks (n = 5), 6 weeks (n = 7), 8 weeks (n = 7), and 10 weeks (n = 19).
 (B) Number of APs fired by $\text{Glut}_{\text{M+FBS}}$ Ns in response to current injection from 0 to 50 pA. AP number $\text{Glut}_{\text{M+FBS}}$ Ns at 2 weeks (n = 12), 4 weeks (n = 48), 6 weeks (n = 65), 8 weeks (n = 56), and 10 weeks (n = 15); AP number $\text{Glut}_{\text{M-FBS}}$ Ns at 2 weeks (n = 6), 4 weeks (n = 4), 6 weeks (n = 7), 8 weeks (n = 5), and 10 weeks (n = 11).
 (C) AP firing types of $\text{Glut}_{\text{M-FBS}}$ Ns. At 8 weeks, most neurons were of the tonic AP firing type ($\text{Glut}_{\text{M+FBS}}$ Ns and $\text{Glut}_{\text{M-FBS}}$ Ns as in A).
 (D) Number of APs fired by $\text{Glut}_{\text{M-FBS}}$ Ns in response to current injection from 0 to 50 pA (AP number $\text{Glut}_{\text{M+FBS}}$ Ns and $\text{Glut}_{\text{M-FBS}}$ Ns as in B).
 (E–G) Passive electrical properties of GlutNs: RMP (E), capacitance (F), and R_{input} (G). RMP $\text{Glut}_{\text{M+FBS}}$ Ns at 2 weeks (n = 19), 4 weeks (n = 57), 6 weeks (n = 80), 8 weeks (n = 60), and 10 weeks (n = 10); $\text{Glut}_{\text{M-FBS}}$ Ns at 2 weeks (n = 4), 4 weeks (n = 4), 6 weeks (n = 7), 8 weeks (n = 6), and 10 weeks (n = 8); capacitance $\text{Glut}_{\text{M+FBS}}$ Ns at 2 weeks (n = 20), 4 weeks (n = 60), 6 weeks (n = 83), 8 weeks (n = 66), and 10 weeks (n = 14); $\text{Glut}_{\text{M-FBS}}$ Ns at 2 weeks (n = 7), 4 weeks (n = 5), 6 weeks (n = 7), 8 weeks (n = 7), and 10 weeks (n = 8); R_{input} $\text{Glut}_{\text{M+FBS}}$ Ns at 2 weeks (n = 18), 4 weeks (n = 55), 6 weeks (n = 62), 8 weeks (n = 52), and 10 weeks (n = 10); $\text{Glut}_{\text{M-FBS}}$ Ns at 2 weeks (n = 6), 4 weeks (n = 4), 6 weeks (n = 7), 8 weeks (n = 8), and 10 weeks (n = 8).
 (H–L) Active electrical properties of GlutNs: AP threshold (H), AP overshoot (I), AP amplitude (J), AP half-width (K), and AHP amplitude (L). $\text{Glut}_{\text{M+FBS}}$ Ns at 2 weeks (n = 12), 4 weeks (n = 49), 6 weeks (n = 66), 8 weeks (n = 53), and 10 weeks (n = 10); $\text{Glut}_{\text{M-FBS}}$ Ns at 2 weeks (n = 6), 4 weeks (n = 4), 6 weeks (n = 7), 8 weeks (n = 6), and 10 weeks (n = 4).
 (M–O) Example traces (top) and current-voltage relationship of I_{K} (M), I_{DR} (N), and I_{A} (O) densities in GlutNs from 2 to 10 weeks.
 (Mii–Oii) Summarized data on densities of peak I_{K} (Mii), I_{DR} (Nii), and I_{A} (Oii). $\text{Glut}_{\text{M+FBS}}$ Ns at 2 weeks (n = 12), 4 weeks (n = 33), 6 weeks (n = 40), 8 weeks (n = 36), and 10 weeks (n = 9); $\text{Glut}_{\text{M-FBS}}$ Ns at 2 weeks (n = 5), 4 weeks (n = 4), 6 weeks (n = 7), 8 weeks (n = 7), and 10 weeks (n = 3).
 (P) Example traces (top) and current-voltage relationship (Pi) and summary graph for densities of peak I_{Na} currents (Pii) in $\text{Glut}_{\text{M+FBS}}$ Ns at 2 weeks (n = 7), 4 weeks (n = 23), 6 weeks (n = 8), and 8 weeks (n = 11).



(legend on next page)

cells differently. $\text{Glut}_{\text{M}+\text{FBS}}$ Ns or $\text{Glut}_{\text{R}+\text{FBS}}$ Ns were fixed and stained for Hsc70 and c-Fos, together with MAP2. Hsc70 is up-regulated in response to various stressors and plays a fundamental role in cell recovery (Klenke et al., 2013). c-Fos was used as an immediate early gene marker to estimate cellular activity (Okuno, 2011). Neurons were stressed by heat shock for 10 min at 45°C and then incubated at 37°C for 90 min to recover (Kotoglou et al., 2009). Hsc70 fluorescence intensity in $\text{Glut}_{\text{R}+\text{FBS}}$ Ns at 8 weeks was 606.9 ± 75.2 a.u., 2-fold higher than in $\text{Glut}_{\text{M}+\text{FBS}}$ Ns (309.4 ± 44.9 a.u.). c-Fos expression was always higher in $\text{Glut}_{\text{R}+\text{FBS}}$ Ns, and c-Fos fluorescence intensity decreased from 532.4 ± 77.1 a.u. at 4 weeks to 124.4 ± 40.3 a.u. at 8 weeks. Decreased cellular activity and elevated stress markers in $\text{Glut}_{\text{R}+\text{FBS}}$ Ns indicate that mouse astrocytes are slightly superior over rat astrocytes for the human neurons (Figure 4).

Furthermore, we assessed the effect of physiologically balanced BrainPhys medium on cultured human neurons (Figures S2H–S2U). Although BrainPhys had been shown to boost synaptic transmission in mass-cultured iPSC-derived human neurons (Bardy et al., 2015), we detected a negative effect on astrocytes in autaptic cultures, with consequent deleterious effects on Glut Ns. Cultures were fixed at 2, 4, 6, and 8 weeks and labeled for GFAP and MAP2. Astrocyte areas cultured in BrainPhys were smaller and astrocytes developed abnormal pointy structures when compared to cells cultured with N3+FBS. Moreover, we noticed an increase of GFAP fluorescence intensity in astrocytes in BrainPhys (Figures S2H–S2J). Once this phenotype had emerged, we cultured cells in N3 me-

dia and replaced it with BrainPhys 5 days before electrophysiological recordings. Here, BrainPhys increased evoked EPSC amplitudes in $\text{Glut}_{\text{M}-\text{FBS}}$ Ns from 0.58 ± 0.09 to 1.00 ± 0.1 nA from 8 to 9 weeks, without significant effects on RRP size, P_{vr} , and mEPSC amplitude or frequency (Figures S2K–S2O). We repeated this experiment with the addition of FBS to the N3 media and again replaced the media with BrainPhys 5 days before experimental recordings. Here, BrainPhys did not enhance synaptic transmission (Figures S2P–S2U). These data show that culturing neurons with mouse astrocytes in the presence of 0.5% FBS is the best choice.

Rapid Maturation of NGN2-Induced Autaptic Human Neurons

To circumvent the long-term culture required for the maturation of classically differentiated human neurons, we used our optimized culture conditions (i.e., mouse astrocytes, N3 medium, and 0.5% FBS) to generate autaptic cultures of human Glut Ns after direct induction with NGN2 (iGlutNs) (Zhang et al., 2013). We first studied the morphology of iGlutNs after 2 and 4 weeks in culture by Sholl analysis (Figures 5A–5C). Cells at 2 weeks already showed pronounced processes, which had grown substantially at 4 weeks (intersections per neuron, 109.7 ± 8.9 at 2 weeks and 167.8 ± 18.0 at 4 weeks; enclosing radius, 131.3 ± 9.2 μm at 2 weeks and 165.8 ± 12.4 μm at 4 weeks). Similarly, the number of synapses, as determined by colabeling VGluT1, Shank2, and MAP2 and quantification as explained earlier, increased from 2 weeks (4.6 ± 1.3 per cell) to 4 weeks (69 ± 10.3 per cell) (Figures 5D and 5E).

Figure 3. Characterization of Synaptic Transmission in Glut_{M} Ns

- (A) Example (top) and mean EPSC amplitudes. $\text{Glut}_{\text{M}+\text{FBS}}$ Ns (black) at 2 weeks (n = 3), 3 weeks (n = 8), 4 weeks (n = 9), 5 weeks (n = 6), 6 weeks (n = 27), 7 weeks (n = 49), 8 weeks (n = 67), 9 weeks (n = 42), 10 weeks (n = 46), and 11 weeks (n = 7); $\text{Glut}_{\text{M}-\text{FBS}}$ Ns (gray) at 2 weeks (n = 1), 4 weeks (n = 2), 6 weeks (n = 7), 7 weeks (n = 3), 8 weeks (n = 11), 9 weeks (n = 7), 10 weeks (n = 7), 11 weeks (n = 5), and 12 weeks (n = 6).
- (B) Mean EPSC potentiation in $\text{Glut}_{\text{M}+\text{FBS}}$ Ns by 3 μM PDBu (n = 11).
- (C) Mean EPSC amplitudes. $\text{Glut}_{\text{R}+\text{FBS}}$ Ns (black) at 6 weeks (n = 2), 7 weeks (n = 18), 8 weeks (n = 16), 9 weeks (n = 15), and 10 weeks (n = 11); $\text{Glut}_{\text{R}-\text{FBS}}$ Ns (gray) at 7 weeks (n = 11), 8 weeks (n = 16), 9 weeks (n = 9), and 10 weeks (n = 6).
- (D) Mean EPSC potentiation in $\text{Glut}_{\text{R}+\text{FBS}}$ Ns by 3 μM PDBu (n = 12).
- (E) Mean RRP sizes. $\text{Glut}_{\text{M}+\text{FBS}}$ Ns at 6 weeks (n = 7), 7 weeks (n = 21), 8 weeks (n = 29), 9 weeks (n = 18), and 10 weeks (n = 28); $\text{Glut}_{\text{M}-\text{FBS}}$ Ns at 6 weeks (n = 3), 7 weeks (n = 2), 8 weeks (n = 6), 9 weeks (n = 4), 10 weeks (n = 4), 11 weeks (n = 4), and 12 weeks (n = 3).
- (F) Mean P_{vr} . $\text{Glut}_{\text{M}+\text{FBS}}$ Ns at 6 weeks (n = 7), 7 weeks (n = 21), 8 weeks (n = 29), 9 weeks (n = 18), and 10 weeks (n = 28); $\text{Glut}_{\text{M}-\text{FBS}}$ Ns at 6 weeks (n = 3), 7 weeks (n = 2), 8 weeks (n = 6), 9 weeks (n = 4), 10 weeks (n = 4), 11 weeks (n = 4), and 12 weeks (n = 3).
- (G) Mean RRP sizes. $\text{Glut}_{\text{R}+\text{FBS}}$ Ns at 7 weeks (n = 5), 8 weeks (n = 11), 9 weeks (n = 6), and 10 weeks (n = 10); $\text{Glut}_{\text{R}-\text{FBS}}$ Ns, 7 weeks (n = 4), 8 weeks (n = 5), 9 weeks (n = 4), and 10 weeks (n = 3).
- (H) Mean P_{vr} . $\text{Glut}_{\text{R}+\text{FBS}}$ Ns at 7 weeks (n = 5), 8 weeks (n = 11), 9 weeks (n = 6), and 10 weeks (n = 10); $\text{Glut}_{\text{R}-\text{FBS}}$ Ns at 7 weeks (n = 4), 8 weeks (n = 5), 9 weeks (n = 4), and 10 weeks (n = 3).
- (I) Mean mEPSC amplitudes. $\text{Glut}_{\text{M}+\text{FBS}}$ Ns at 6 weeks (n = 6), 7 weeks (n = 18), 8 weeks (n = 28), 9 weeks (n = 13), and 10 weeks (n = 29); $\text{Glut}_{\text{M}-\text{FBS}}$ Ns at 6 weeks (n = 3), 8 weeks (n = 4), 9 weeks (n = 2), 10 weeks (n = 3), 11 weeks (n = 4), and 12 weeks (n = 2).
- (J) Mean mEPSC frequencies. $\text{Glut}_{\text{M}+\text{FBS}}$ Ns at 6 weeks (n = 6), 7 weeks (n = 18), 8 weeks (n = 28), 9 weeks (n = 13), and 10 weeks (n = 29); $\text{Glut}_{\text{M}-\text{FBS}}$ Ns at 6 weeks (n = 3), 8 weeks (n = 4), 9 weeks (n = 2), 10 weeks (n = 3), 11 weeks (n = 4), and 12 weeks (n = 2).
- (K) Mean mEPSC amplitudes. $\text{Glut}_{\text{R}+\text{FBS}}$ Ns at 7 weeks (n = 5), 8 weeks (n = 6), 9 weeks (n = 5), and 10 weeks (n = 9); $\text{Glut}_{\text{R}-\text{FBS}}$ Ns at 7 weeks (n = 2), 8 weeks (n = 5), 9 weeks (n = 2), and 10 weeks (n = 2).
- (L) Mean mEPSC frequencies. $\text{Glut}_{\text{R}+\text{FBS}}$ Ns at 7 weeks (n = 5), 8 weeks (n = 6), 9 weeks (n = 5), and 10 weeks (n = 9); $\text{Glut}_{\text{R}-\text{FBS}}$ Ns at 7 weeks (n = 2), 8 weeks (n = 5), 9 weeks (n = 2), and 10 weeks (n = 2).
- (M) STP of $\text{Glut}_{\text{M}+\text{FBS}}$ Ns at 5 Hz (n = 36), 10 Hz (n = 87), and 40 Hz (n = 61) and of $\text{Glut}_{\text{M}-\text{FBS}}$ Ns at 10 Hz (n = 15) and 40 Hz (n = 7).
- (N) STP of $\text{Glut}_{\text{R}+\text{FBS}}$ Ns at 5 Hz (n = 29), 10 Hz (n = 27), and 40 Hz (n = 27) and of $\text{Glut}_{\text{R}-\text{FBS}}$ Ns at 5 Hz (n = 9), 10 Hz (n = 7), and 40 Hz (n = 7).
- (O) Diagram and representative traces of double 40 Hz stimulation with different time intervals, and plot of the cumulative charge transfer curve (arrowhead indicates the y intercept).
- (P) EPSC (black) and RRP (gray) recovery ratios of $\text{Glut}_{\text{M}+\text{FBS}}$ Ns (all n = 10).
- Insets in (A), (C), (E), and (G) show representative traces ($\text{Glut}_{\text{M}+\text{FBS}}$ Ns: 4 weeks, red; 6 weeks, blue; 8 weeks black; $\text{Glut}_{\text{M}-\text{FBS}}$ Ns: 8 weeks, gray). Insets in (B) and (D) show representative traces before (black) and during PDBu (blue) application. Insets in (I) and (J) show representative mEPSC traces.

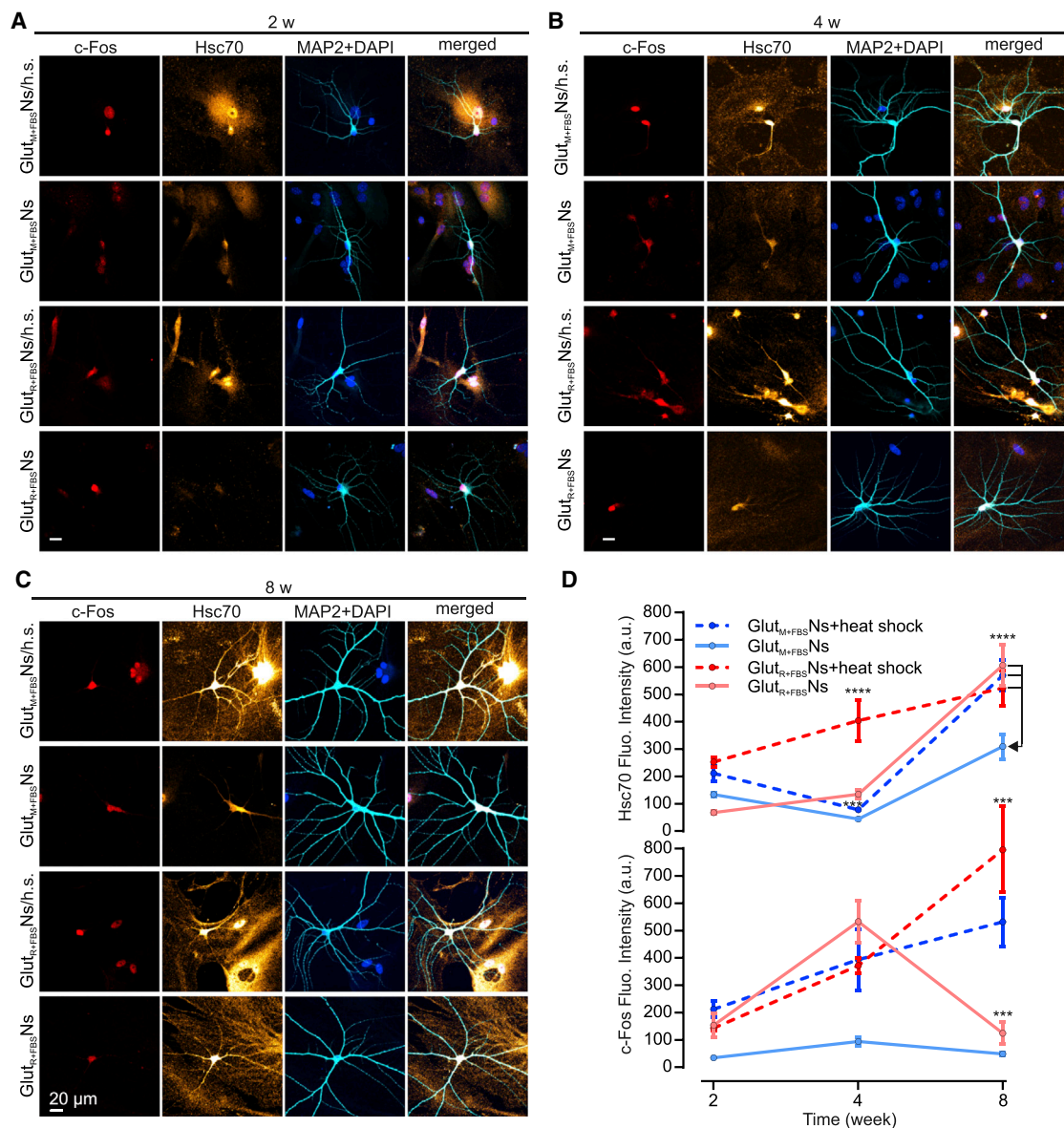


Figure 4. Astrocyte Types and Culture Media Affect Cell Stress in GlutNs

GlutNs were co-cultured with either rat or mouse astrocytes and cultured with or without FBS. Cells were fixed at different time points and stained against the cell activity marker c-Fos and the cell stress marker Hsc70, together with MAP2 and DAPI labeling.

(A–C) Representative confocal images of GlutNs stained against c-Fos (red), Hsc70 (orange hot), and MAP2 (cyan), as well as with DAPI (blue), fixed at 2 (A), 4 (B), and 8 (C) weeks, respectively.

(D) Hsc70 and c-Fos fluorescence intensity levels as a function of time under the different culturing conditions. Hsc70 signal intensity was measured across the cell body, and c-Fos intensity was quantified across the nucleus. At 2, 4, and 8 weeks, respectively, $n = 17, 16,$ and 17 (M+FBS/heat shock); $n = 16, 17,$ and 15 (M+FBS); $n = 17, 20,$ and 16 (R+FBS/heat shock); and $n = 16, 20,$ and 17 (R+FBS).

One-way ANOVA test was applied (** $p < 0.001$, **** $p < 0.0001$).

At 2 weeks, iGlutNs showed robust EPSCs (0.67 ± 0.16 nA), which increased to ~ 1.5 nA at 4 weeks (Figure 5F). The parallel increase of the RRP over development was more uniformly continuous (0.03 ± 0.01 nC at 2 weeks to 0.12 ± 0.03 nC at 4 weeks) (Figure 5H), so the calculated P_{vr} was $8.5\% \pm 2.1\%$ at 2 weeks versus $6.6\% \pm 0.8\%$ at 4 weeks (Figure 5I). mEPSC amplitudes were stable around 33 pA over development, while

mEPSC frequencies increased continuously from 1.3 Hz at 2 weeks to 3.1 Hz at 4 weeks (Figures 5J and 5K). PDBu increased EPSCs by ~ 1.4 -fold (Figure 5G), similar to GlutNs. Thus, basic synaptic features of iGlutNs were similar to those of GlutNs. Furthermore, features of STP, paired-pulse ratio (PPR), and EPSC and RRP recovery in iGlutNs (Figures 5L and 5M) were qualitatively similar to those of GlutNs (Figures 3M–3P) and

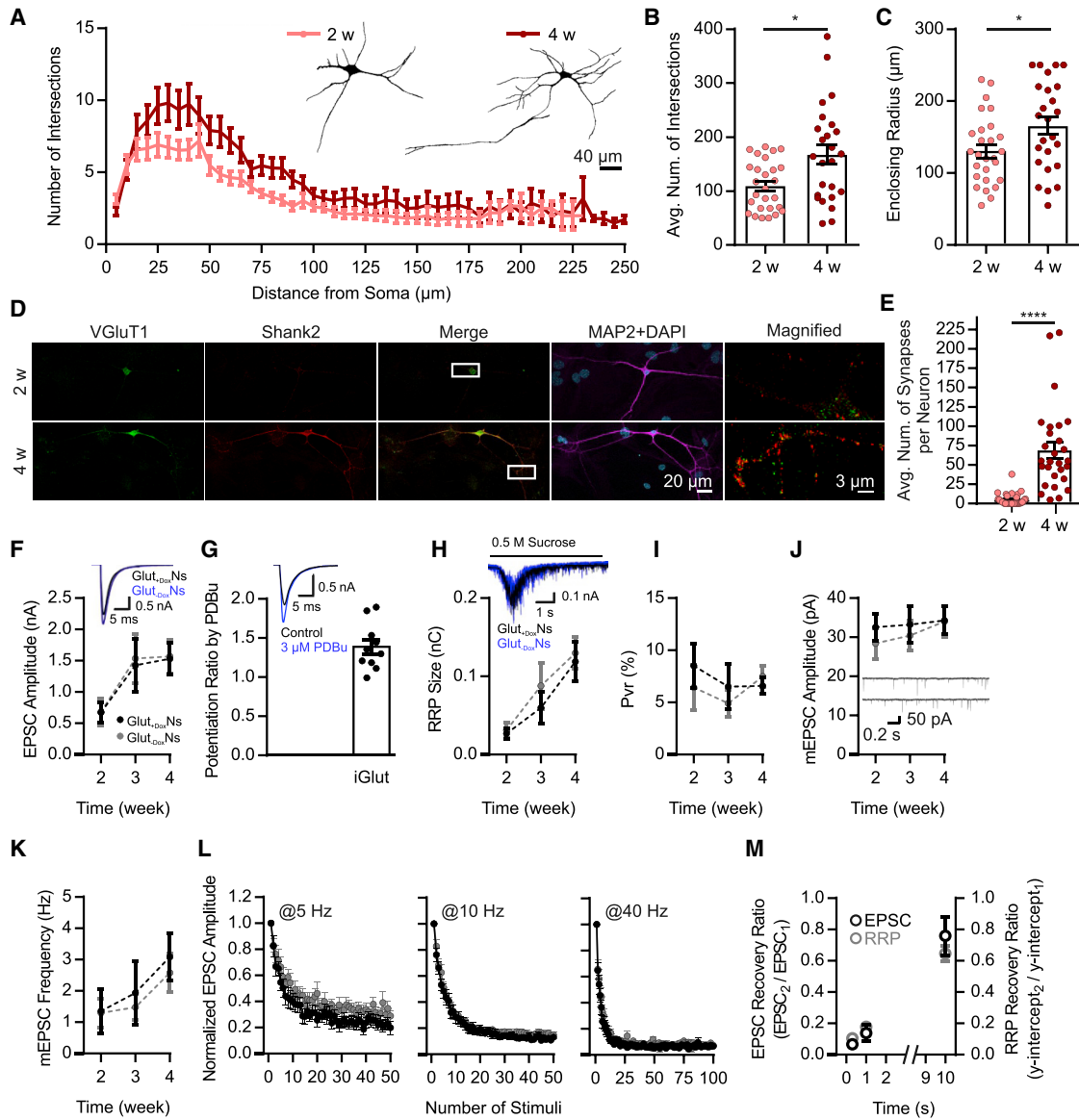


Figure 5. Characterization of Morphological and Functional Properties of iGlutNs

(A) Number of dendritic intersections of iGlutNs (2 weeks and 4 weeks) plotted as a function of distance from the soma. Binarized images in insets show iGlutNs at 2 weeks (left) and 4 weeks (right).

(B) Average number of dendrites intersecting Sholl circles 5–250 μm from the soma as a function of time.

(C) Enclosing radius of dendrites measured from the soma. iGlutNs at 2 weeks ($n = 27$) and 4 weeks ($n = 25$).

(D) Confocal images of iGlutNs at 2 and 4 weeks (top and bottom panels, respectively). Antigens and stains are indicated.

(E) Average number of synapses per neuron at 2 weeks ($n = 36$) and 4 weeks ($n = 29$).

(F) Mean EPSC amplitudes. iGlut_{+Dox}Ns (black) at 2 weeks ($n = 18$), 3 weeks ($n = 18$), and 4 weeks ($n = 42$); iGlut_{-Dox}Ns (gray) at 2 weeks ($n = 15$), 3 weeks ($n = 15$), and 4 weeks ($n = 33$).

(G) Mean EPSC potentiation in iGlut_{+Dox}Ns by 3 μM PDBu ($n = 10$).

(H) Mean RRP sizes. iGlut_{+Dox}Ns at 2 weeks ($n = 6$), 3 weeks ($n = 9$), and 4 weeks ($n = 20$); iGlut_{-Dox}Ns at 2 weeks ($n = 7$), 3 weeks ($n = 6$), and 4 weeks ($n = 12$).

(I) Mean P_vr. iGlut_{+Dox}Ns at 2 weeks ($n = 6$), 3 weeks ($n = 9$), and 4 weeks ($n = 20$); iGlut_{-Dox}Ns at 2 weeks ($n = 7$), 3 weeks ($n = 6$), and 4 weeks ($n = 12$).

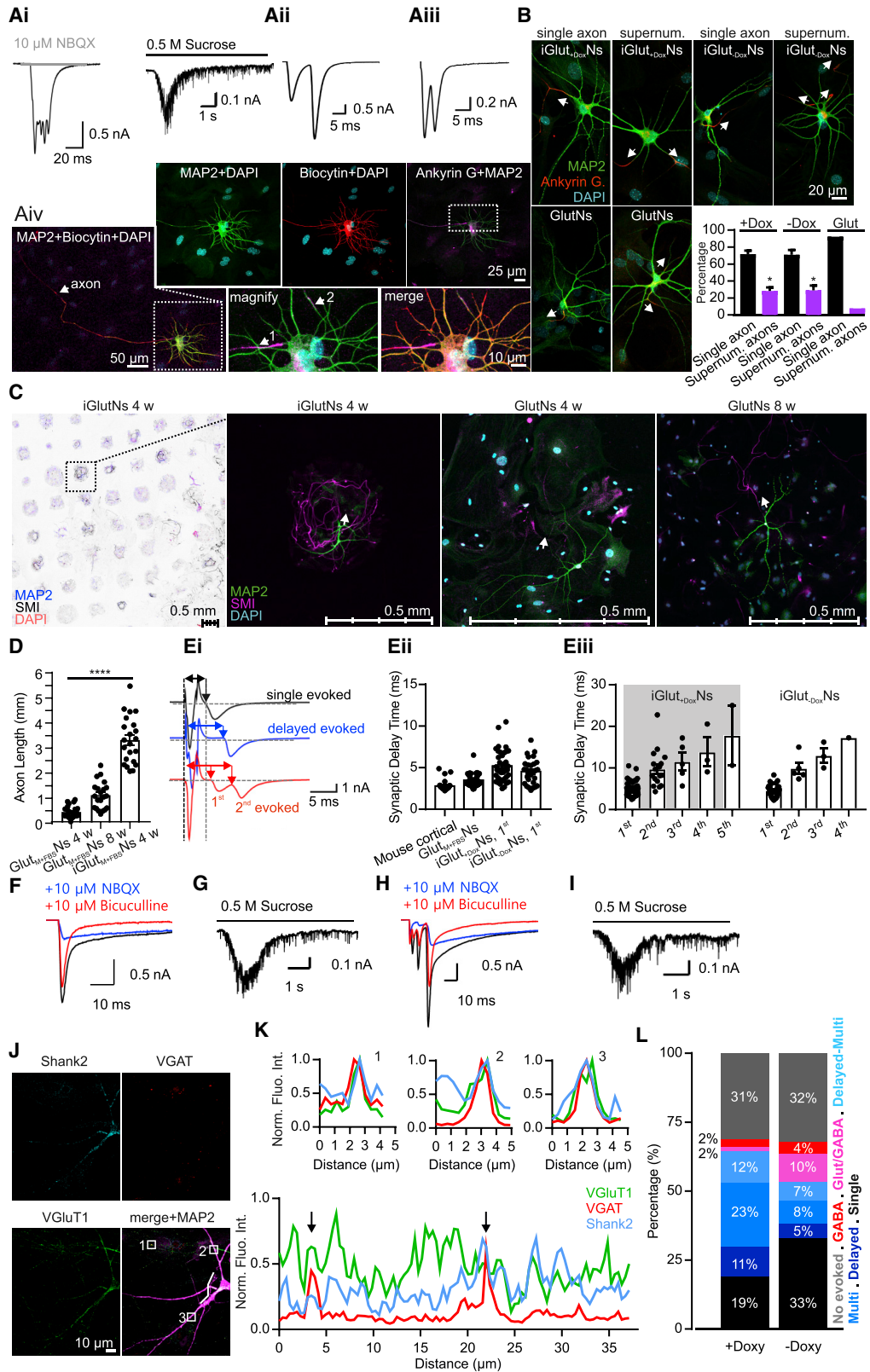
(J) Mean mEPSC amplitudes. iGlut_{+Dox}Ns at 2 weeks ($n = 6$), 3 weeks ($n = 5$), and 4 weeks ($n = 12$); iGlut_{-Dox}Ns at 2 weeks ($n = 10$), 3 weeks ($n = 6$), and 4 weeks ($n = 10$).

(K) Mean mEPSC frequencies. iGlut_{+Dox}Ns at 2 weeks ($n = 6$), 3 weeks ($n = 5$), and 4 weeks ($n = 12$); iGlut_{-Dox}Ns at 2 weeks ($n = 10$), 3 weeks ($n = 6$), and 4 weeks ($n = 10$).

(L) STP of iGlut_{+Dox}Ns at 5 Hz ($n = 12$), 10 Hz ($n = 21$), and 40 Hz ($n = 21$) and of Glut_{-Dox}Ns at 5 Hz ($n = 13$), 10 Hz ($n = 21$), and 40 Hz ($n = 16$).

(M) EPSC (black) and RRP (gray) recovery ratios of iGlut_{+Dox}Ns (all $n = 10$).

Insets in (F)–(H) show representative traces (+Dox/control, black; –Dox/PDBu, blue). Mann-Whitney test was applied (* $p < 0.05$, **** $p < 0.0001$).



(legend on next page)

mouse cortical neurons (Figures S6S and S6T). However, STD and paired pulse depression were more pronounced in iGluTNs.

Because doxycycline (Dox) is used to induce NGN2 expression, we assessed whether continued Dox treatment affects iGluTNs. None of the tested parameters were different between iGluT₊DoxNs and iGluT₋DoxNs (Figures 5F–5M), indicating that Dox presence does not affect the maturation and function of iGluTNs after initial induction.

We tested an additional iGluTN line (C35) and compared key features with the routinely used C14 line. Passive membrane properties, AP characteristics, EPSC amplitudes, and STD were strikingly similar between the two lines (Figures S4A–S4E), demonstrating that our culture system leads to reliable and reproducible readouts even from two different cell lines.

Unusual Morphological and Functional Features of NGN2-Induced Neurons

NGN2-induced neurons have the clear advantage of rapid maturation. However, this rapid maturation may lead to unusual developmental trajectories, although earlier studies did not detect abnormalities (Zhang et al., 2013).

We consistently detected unusual multi-peak EPSCs in a subset of single autaptic iGluTNs (Figure 6A). We first used hypertonic sucrose stimulation to test whether multi-peak EPSCs might be due to more than one neuron present, expecting sucrose responses combined with an AP-like spike response, which was never observed (Figure 6Ai). To test whether multi-peak EPSCs might originate from cells with multiple axons, we filled patched neurons with 0.2% biocytin, stained them using streptavidin and antibodies to MAP2 and Ankyrin G (marker of axon initial segments) (Figure 6Aiv), and found that double EPSC peaks corresponded to cells with two or more axons. Regardless of Dox presence, this phenotype was found in about a quarter of all iGluTNs (iGluT₊Dox, 28% ± 2%, and iGluT₋Dox, 29% ± 4%), while only 8% GluT_{M+FBS}Ns showed multiple axons (Figure 6B). Moreover, axons of iGluTNs were longer than those of GluT_{M+FBS}N

axons, as assessed by staining iGluTNs at 4 weeks and GluT_{M+FBS}Ns at 4 and 8 weeks for SMI-312 (axons) and MAP2 (iGluT at 4 weeks, 3.7 ± 0.1 mm; GluT_{M+FBS} at 4 weeks, 0.53 ± 0.04 mm; and GluT_{M+FBS} at 8 weeks, 1.3 ± 0.1 mm) (Figures 6C and 6D). Given the length of iGluTN axons and their small diameter, multi-peak EPSCs with inter-peak intervals of 2–5 ms are conceivable. We further tested whether the long iGluTNs axons also cause longer delays between AP and EPSC onsets (Figure 6Ei). GluT_{M+FBS}Ns showed slightly longer synaptic delays compared with mouse cortical neurons, and the delay was more pronounced in iGluT₊Dox/-DoxNs (3.47 ± 0.11, 5.18 ± 0.3, and 4.54 ± 0.2 ms, respectively) (Figures 6Eii and S4). The presence of Dox did not affect the synaptic delay (Figure 6Eiii).

Apart from multi-peak EPSCs, some iGluTNs showed unusual EPSC kinetics with a pronounced slow component indicative of a GABAergic contribution. When we applied the GABA_A receptor antagonist bicuculline or the α -amino-3-hydroxy-5-methyl-4-isoxazolepropionic acid (AMPA) receptor antagonist NBQX, the former blocked the slow EPSC component while the latter blocked the fast one (Figures 6F–6I), indicating corelease of GABA and glutamate by individual iGluTNs. Accordingly, staining of VGAT (a GABAergic presynapse marker) and VGluT1 (a Glut-presynapse marker), along with labeling of Shank2 and MAP2, showed that some iGluTNs coexpress VGAT and VGluT1 at the same synapses (Figures 6J–6L).

Human Inhibitory Neurons in Autaptic Culture

Because GABAergic dysfunction is implicated in many brain diseases, we devised autaptic culture methods for iPSC-derived GABAergic neurons, comparing rat versus mouse astrocytes and the presence versus the absence of FBS in the media. We started with GABANs and analyzed a subset of electrophysiological parameters. Evoked inhibitory postsynaptic currents (IPSCs) were found in GABA_{M+FBS}Ns by 3 weeks and increased to ~1.2 nA by 7 to 9 weeks. GABA_{M-FBS}Ns behaved similarly, with further increases of IPSC amplitudes until 13 weeks

Figure 6. Unusual Properties of iGluTNs in Autaptic Culture

(A) Representative EPSC and sucrose traces of iGluTNs with supernumerary axons (Ai–Aiii). To correlate electrophysiology with morphological analysis, patched iGluTNs were filled with biocytin and stained against Ankyrin G and MAP2, along with DAPI. (Aiv) Representative image of a biocytin-filled neuron. Insets show MAP2+DAPI, biocytin+DAPI, and Ankyrin G+MAP2 labeling and magnified and merged images.

(B) Immunofluorescence images of GluTNs and iGluTNs with or without Dox, stained at 4 weeks against Ankyrin G (red) and MAP2 (green), as well as with DAPI (cyan). The adjacent graph shows the percentage of cells with single and supernumerary axons in iGluTNs, iGluT₋DoxNs, and GluTNs (iGluT₊DoxNs, n = 121; iGluT₋DoxNs, n = 56; GluTNs, n = 44).

(C) First panel: representative overview of stamped micro-islands with cells stained against MAP2 and SMI-312, as well as with DAPI. Second panel: iGluTNs cells fixed at 4 weeks. Third and fourth panels: GluT cells fixed at 4 and 8 weeks, respectively.

(D) Axon length of GluTNs at 4 weeks (n = 26) and 8 weeks (n = 21) and iGluTNs at 4 weeks (n = 22).

(E) Diagram of synaptic delay measurements and representative traces of three evoked EPSC types (single evoked, black; delayed evoked, blue; delayed-multiple evoked, red) (Ei). (Eii) Comparison of synaptic delay in mouse forebrain cortical neurons (n = 29), GluT_{M+FBS}Ns at 8 weeks (n = 44), and iGluT₊DoxNs (n = 39) and iGluT₋DoxNs (n = 30). In iGluTNs, the first evoked response was used to measure synaptic delay. (Eiii) Synaptic delay of iGluT₊DoxNs at the 1st (n = 39), 2nd (n = 17), 3rd (n = 5), 4th (n = 3), and 5th (n = 2) EPSC and of iGluT₋DoxNs at the 1st (n = 30), 2nd (n = 5), 3rd (n = 3), and 4th (n = 1) EPSC.

(F–I) Representative traces of corelease of glutamate and GABA by iGluTNs (F and H) and sucrose responses (G and I). Pharmacologically untreated EPSCs, black; inhibition of GABA responses (10 μ M bicuculline), red; inhibition of glutamate responses (10 μ M NBQX), blue.

(J and K) iGluTN samples were fixed and stained against VGAT, VGluT1, Shank2, and MAP2 (J). Exemplary line scans were plotted, and normalized fluorescence intensities are shown in the adjacent graphs (K). Black arrows indicate synapses with VGluT1 and VGAT signals (K). White squares indicate individual synapses with VGAT and VGluT1 signals (J).

(L) Percentages of iGluT₊DoxNs and iGluT₋DoxNs with different types of evoked release. For iGluT₊DoxNs and iGluT₋DoxNs, respectively: non-responders, gray (n = 38 and 38); GABA release, red (n = 3 and 5); corelease, pink (n = 2 and 12); delayed-multiple evoked, light blue (n = 14 and 8); multiple evoked, blue (n = 28 and 10); delayed evoked, navy (n = 13 and 6); single evoked, black (n = 23 and 39).

Kruskal-Wallis test (B) and one-way ANOVA (D) were applied (*p < 0.05, ****p < 0.0001).

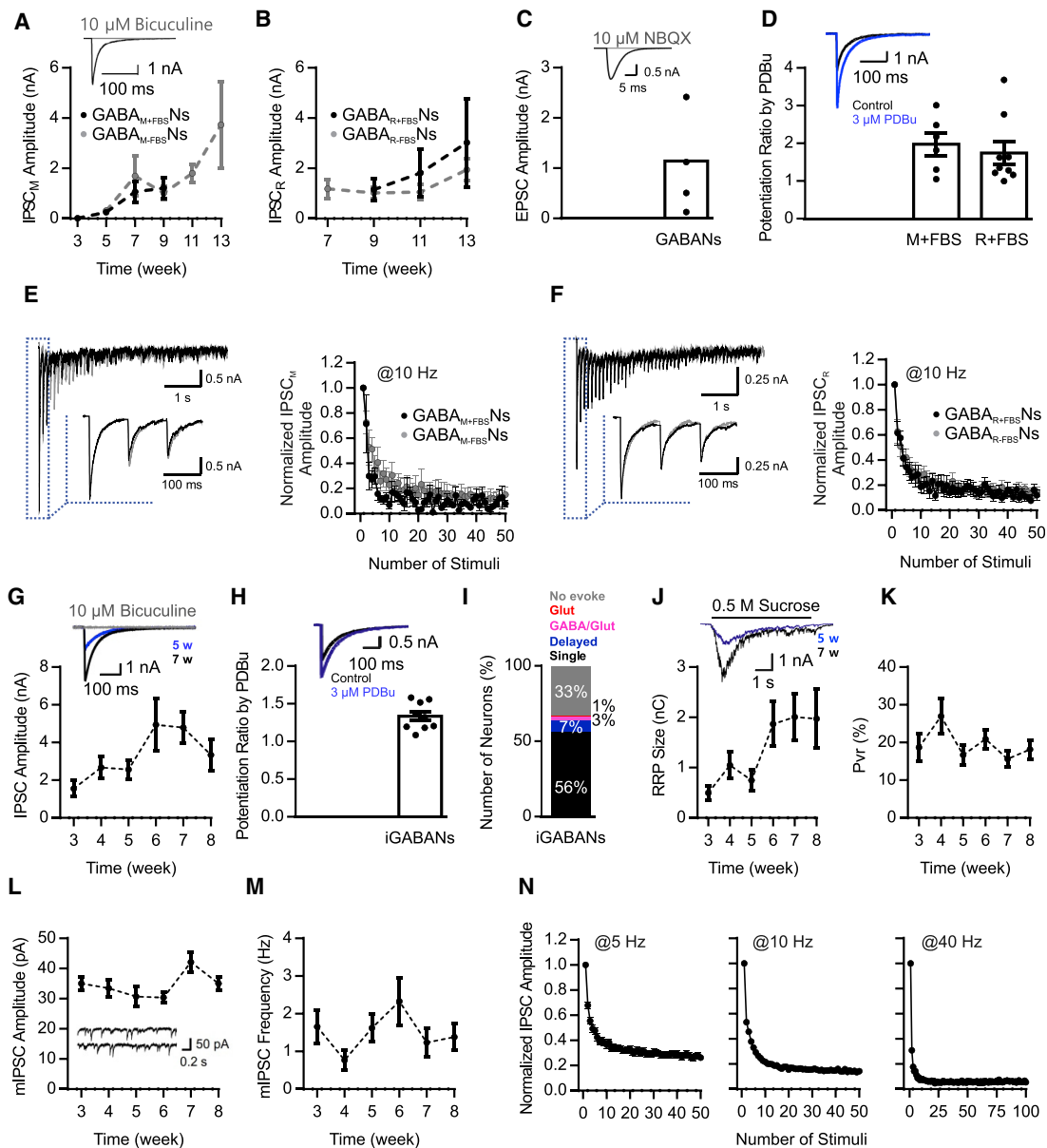


Figure 7. Characterization of Synaptic Transmission in GABANs and iGABANs

(A) Mean IPSC amplitudes. GABA_{M+}FBSNs (black) at 3 weeks (n = 6), 5 weeks (n = 8), 7 weeks (n = 7), and 9 weeks (n = 10); GABA_{M-}FBSNs (gray) at 5 weeks (n = 11), 7 weeks (n = 3), 9 weeks (n = 23), 11 weeks (n = 28), and 13 weeks (n = 3).

(B) Mean IPSC amplitudes. GABA_{R+}FBSNs (black) at 9 weeks (n = 12), 11 weeks (n = 3), and 13 weeks (n = 5); GABA_{R-}FBSNs (gray) at 7 weeks (n = 14), 9 weeks (n = 37), 11 weeks (n = 24), and 13 weeks (n = 17).

(C) EPSC amplitudes in a small subset of all tested GABANs (n = 4).

(D) Mean IPSC potentiation in GABA_{M+}FBSNs (n = 6) and GABA_{R+}FBSNs (n = 9) by 3 μ M PDBu.

(E) Representative trace of STD in GABA_{M+}FBSNs (black) and GABA_{M-}FBSNs (gray) during 10 Hz stimulation (left), and STP (at 7–9 weeks, GABA_{M+}FBSNs, n = 6; GABA_{M-}FBSNs, n = 8) (right). The inset shows the first three episodes of the train.

(F) Representative trace of STD in GABA_{R+}FBSNs (black) and GABA_{R-}FBSNs (gray) during 10 Hz stimulation (left), and STP (at 7–9 weeks, GABA_{R+}FBSNs, n = 9; GABA_{R-}FBSNs, n = 13). The inset shows the first three episodes of the train.

(G) Mean IPSC amplitudes. iGABANs at 3 weeks (n = 16), 4 weeks (n = 14), 5 weeks (n = 17), 6 weeks (n = 9), 7 weeks (n = 17), and 8 weeks (n = 23).

(H) Mean IPSC potentiation in iGABANs by 3 μ M PDBu (n = 9).

(I) Percentages of iGABANs with different types of evoked release. Single evoked, black (n = 86); delayed evoked, navy (n = 11); corelease, pink (n = 4); glutamate release, red (n = 2); non-responders, gray (n = 50).

(J) Mean RRP sizes. iGABANs at 3 weeks (n = 12), 4 weeks (n = 10), 5 weeks (n = 12), 6 weeks (n = 6), 7 weeks (n = 14), and 8 weeks (n = 17).

(K) Mean P_vr. iGABANs at 3 weeks (n = 12), 4 weeks (n = 10), 5 weeks (n = 12), 6 weeks (n = 6), 7 weeks (n = 14), and 8 weeks (n = 17).

(legend continued on next page)

(3.7 ± 1.7 nA, not measured in GABA_{M+FBS}Ns) (Figure 7A). GABA_RNs were only assayed from 7 to 13 weeks. IPSC amplitudes increased in GABA_{R+FBS}Ns between 9 and 13 weeks to 3.0 ± 1.7 nA, while GABA_{R-FBS}N IPSCs remained rather stable around 1.1–1.9 nA (Figure 7B). GABA_{M+FBS/M-FBS}Ns were pure, with only 0.7% of analyzed cells exhibiting a Glut phenotype (Figure 7C). Furthermore, IPSCs in GABA_{M+FBS}Ns (7–8 weeks) and GABA_{R+FBS}Ns (8 weeks) increased similarly in response to PDBu treatment (1.75- to 1.97-fold) (Figure 7D), and GABA_MNs and GABA_RNs showed similar STD time courses during high-frequency stimulation, irrespective of the presence or absence of FBS (Figures 7E and 7F). Overall, these data show that GABANs in autaptic culture, unlike GlutNs, are rather insensitive to the astrocyte type and to FBS in the culture medium.

iGABANs induced by ASCL1 and DLX2 (Yang et al., 2011) on mouse astrocytes (in N3 medium with 0.5% FBS) developed faster than GlutNs, much like iGlutNs. From 2 to 8 weeks in culture, iGABANs were mostly of the tonic AP firing type (Figures S5A and S5B). They had a stable RMP of about -50 mV over time in culture, increased in size as assessed by cell capacitance from 2 weeks (~ 18 pF) to a plateau at 6 weeks (~ 36 pF) (about half the size of corresponding GlutNs and iGlutNs), and showed a progressive decrease in R_{input} from 2 weeks ($\sim 1,200$ M Ω) to stabilize at 6 weeks (~ 700 M Ω) (Figures S5C–S5E). AP threshold (-17 to -24 mV), overshoot (38 to 50 mV), amplitude (60 to 67 mV), and width (1.5 to 2.4 ms) remained rather stable over time in culture, while AHP increased from -16 mV at 2 weeks to -24 mV at 8 weeks (Figures S5F–S5J). Like iGlutNs (Figures S4R–S4T), iGABANs had higher I_K , I_{DR} , and I_A densities (Figures S5K–S5M) than GlutNs (Figures 2M–2O), indicating that the degree of differentiation correlates with I_K , I_{DR} , and I_A density. iGABANs grew rapidly from 2 to 4 weeks and then gradually increased in size and complexity until 8 weeks (Figures S5N–S5Q). Synaptic currents in iGABANs first appeared at 3 weeks, after which IPSC amplitudes gradually increased to 4.95 ± 1.38 nA at 6 weeks; beyond 7 weeks, IPSC amplitudes decreased again (Figure 7G). In accordance with changes in IPSC amplitudes with time, the number of inhibitory synaptic puncta also increased (Figure S5R).

PDBu caused a slight (1.34-fold) increase in IPSC amplitudes (Figure 7H). More than 50% of cells showed single IPSCs in response to single APs, about 30% of cells did not show synaptic responses, 7.2% displayed delayed synaptic responses, and 3% showed GABA and glutamate corelease (Figure 7I). The RRP size increased from ~ 0.5 nC at 3 weeks to 1.87 ± 0.44 nC at 6 weeks and then remained steady (Figure 7J). Correspondingly, the P_{vr} remained relatively stable over time (Figure 7K). Miniature inhibitory postsynaptic current (mIPSC) amplitudes were generally stable throughout the culturing period, with some fluctuation at 7 weeks (30–42 pA), while mIPSC frequencies fluctuated substantially during culture time (Figures 7L and 7M). Finally,

iGABANs showed strong STD at stimulation frequencies of 5–40 Hz (Figure 7N).

DISCUSSION

Cell cultures are commonplace in all areas of biomedical research. They are used as reductionist experimental systems despite certain disadvantages, such as loss of tissue context, because of their low complexity, reproducibility, amenability to manipulations, and high-throughput potential. In neuroscience, thousands of studies have employed primary neuron cultures, mostly from rodents, to discover new biology—from basic principles to disease mechanisms. However, the usefulness of cultured rodent neurons reaches its limits in the context of neurological and psychiatric brain diseases. Many of these have a substantial genetic etiology, but modeling corresponding genetic disease causes is often impossible because of their multigenic nature. Furthermore, intrinsic differences between rodent and human neurons may limit the interpretability of data. Here, the advent of methods to generate human neurons from iPSCs of probands (Okita and Yamanaka, 2011; Takahashi and Yamanaka, 2016; Yang et al., 2017) and to rapidly manipulate them genetically (Doudna and Charpentier, 2014) heralds a revolution. Systematic analyses of patient-derived neurons are possible and hold great promise, because the genetic disease causes manifest at the cellular level.

In terms of standardized, systematic analyses of morphological, biophysical, and synaptic properties of wild-type and mutant neurons with efficient throughput, the autaptic culture system with single neurons on small astrocyte feeder islands is particularly useful, because it combines easy experimental access to cells and the potential to read out a plethora of cellular features with standardization, reproducibility, and medium-throughput potential (Bekkers and Stevens, 1991; Pyott and Rosenmund, 2002; Burgalossi et al., 2012). Even single experimenters can electrophysiologically characterize dozens of autaptic cells in a few days, and inter-laboratory differences are typically so small that datasets can be combined to deduce biological principles (Schotten et al., 2015).

We optimized the autaptic culture system for human iPSC-derived neurons, i.e., classically differentiated GlutNs and GABANs, as well as iGlutNs and iGABANs, both induced by forced transcription factor expression. GlutNs and GABANs were used to determine optimal media compositions, astrocyte origin, and FBS supplementation. N3 medium with 0.5% FBS and mouse astrocytes turned out to be optimal. In BrainPhys, micro-island astrocytes were smaller and showed unusual morphology and increased GFAP immunofluorescence, with deleterious effects on cultured neurons. Furthermore, it did not improve functional readouts when used after an initial culturing phase in N3 medium with 0.5% FBS. Our medium, however, improved cell survival, maturation, and functionality under

(L) Mean mIPSC amplitudes. iGABANs at 3 weeks (n = 11), 4 weeks (n = 11), 5 weeks (n = 12), 6 weeks (n = 6), 7 weeks (n = 13), and 8 weeks (n = 15).

(M) Mean mIPSC frequencies. iGABANs at 3 weeks (n = 11), 4 weeks (n = 11), 5 weeks (n = 12), 6 weeks (n = 6), 7 weeks (n = 13), and 8 weeks (n = 15).

(N) STP of iGABANs at 5 Hz (n = 38), 10 Hz (n = 79), and 40 Hz (n = 78).

Insets in (A) and (C) show representative PSP traces with (gray) and without (black) blockers. Insets in (D) and (H) show representative IPSC traces before (black) and during (blue) 3 μ M PDBu application. Insets in (G) and (J) show representative traces at 5 weeks (blue) and at 7 weeks (black).

almost all conditions tested. FBS had the strongest positive effect on the maturation of synaptic functionality, while cell sizes and membrane properties were less affected or unaffected, indicating that these parameters are under strong cell-intrinsic control. The human astrocyte cell line we used was unsuitable for human autapses, because cells died beyond 4 weeks. This may be different with altered culture conditions (or human primary astrocytes), but further optimization was not deemed necessary, because mouse and rat astrocytes supported the growth, maturation, and analysis of human autapses in long-term cultures. Because rat astrocytes were slightly less supportive, e.g., regarding neuronal survival and AP maturation, and caused higher neuronal stress, we propose that mouse astrocytes are optimal for human autaptic cultures. By using N3 media with 0.5% FBS and mouse astrocytes, we found that inter-experimental variations of cellular parameters were small, indicating that we developed consistent and reproducible autaptic culture conditions.

GlutNs and GABANs were pure in terms of transmitter type but took at least 8 weeks (GlutNs) and up to 13 weeks (GABANs) in culture to mature. They showed robust PSCs and STP features that are comparable to those of iGlutNs and mouse cortical neurons, as well as to iGABANs and mouse striatal GABAergic neurons (Nair et al., 2013). Furthermore, GlutNs were mostly of the tonic AP firing type at 8 weeks and showed EPSC and RRP recovery features that were similar to those of mouse cortical neurons. The latter finding indicates that activity-dependent synaptic vesicle recycling operates similarly in synapses of human and rodent neurons.

iGlutNs and iGABANs have the clear advantage of faster maturation, and our gene editing approach enables highly controlled neuronal induction via standardized inducible transcription factor expression from the AAVS1 safe-harbor locus. Key synaptic parameters in iGlutNs stabilized by 3 weeks, while iGABANs took slightly longer to mature. A large proportion of iGlutNs (60%–70%) showed synaptic responses. They were pure regarding transmitter type and almost all iGlutNs were of the tonic AP firing type. Their STP and EPSC and RRP recovery features were similar to those of mouse cortical neurons. However, they displayed somewhat small EPSC amplitudes. Substantial subpopulations of iGlutNs showed multiple and long axons, and some a mixed Glut and GABAergic transmitter phenotype. These unusual properties, whose causes remain unknown, are not confounding the use of iGlutNs as cellular model system because they can be detected easily, but they need to be considered in corresponding analyses. In any case, the long axons of iGlutNs and their multiple axon phenotype cause unusual synaptic delays and multi-peak EPSCs, so cells had to be separated into groups for functional analyses. Like iGlutNs, iGABANs were pure in terms of transmitter type. More than 50% of iGABANs showed synaptic responses, and almost all were of the tonic AP firing type. Their STP features were comparable to those of GABANs and mouse striatal GABAergic neurons (Nair et al., 2013). iGABANs showed no multi-peak IPSCs, indicating that they usually do not have multiple axons.

All human neuron types we tested can be used for standardized and systematic functional studies in autaptic cultures, e.g., in the context of patient-derived cells or human cells with

targeted mutations. Overall, the tested cell types were pure with regard to transmitter type, and surprisingly large fractions of cells showed a tonic AP firing type, indicating that the autapse culture system may promote neuronal maturation or even select for mature cells. As far as direct comparisons of parameters are possible (e.g., with normalized readouts of STP and PSC/RRP recovery), the different related cell types (i.e., GlutNs versus iGlutNs, GABANs versus iGABANs, Glut/iGlutNs versus mouse cortical neurons, and GABA and iGABANs versus mouse striatal neurons) showed similar features, which was also true for a comparison of two iGlutN lines (C14m versus C35m). These findings indicate that the autaptic culture system may eliminate some sources of heterogeneity among iPSC-derived neurons and may thus be useful for future analyses of disease-relevant neurons.

STAR★METHODS

Detailed methods are provided in the online version of this paper and include the following:

- KEY RESOURCES TABLE
- CONTACT FOR REAGENT AND RESOURCE SHARING
- EXPERIMENTAL MODEL AND SUBJECT DETAILS
 - iPSCs - source and generation
 - Mouse maintenance
- METHOD DETAILS
 - Differentiation of iPSCs into glutamatergic cortical neurons
 - Differentiation of iPSCs into GABAergic forebrain neurons
 - Plasmid cloning for forward programming
 - iPSC nucleofection for AAVS1 targeting
 - Forward programming of iPSCs into GABAergic forebrain neurons
 - Cryopreservation of post-mitotic neurons
 - Immunostaining of immature neuronal batches
 - Preparation of astrocyte micro-island cultures
 - Mouse forebrain cortical neuron culture
 - Recovery and culture of cryopreserved human iPSC-derived neurons
 - Immunofluorescence staining and imaging
 - Electrophysiology
- QUANTIFICATION AND STATISTICAL ANALYSIS

SUPPLEMENTAL INFORMATION

Supplemental Information can be found online at <https://doi.org/10.1016/j.celrep.2019.04.059>.

ACKNOWLEDGMENTS

We thank Su-Chun Zhang for providing the AAVS1 targeting vector and corresponding TALEN plasmids. We gratefully acknowledge Tamara Bechler for technical support. Funding sources were the European Commission (H2020, Comorbidity and Synapse Biology in Clinically Overlapping Psychiatric Disorders, Project ID 667301 to O.B., J.S.R., and N.B.) and the German Federal Ministry of Education and Research (Framework of the e:Med Research and Funding Concept, 01ZX1314A-IntegraMent to O.B.; ERA-NET Neuron SynPathy to N.B.).

AUTHOR CONTRIBUTIONS

J.S.R., O.B., and N.B. conceived the study. K.R., T.K., and M.H. generated and analyzed human iPSC-derived neurons; H.J.R. and C.L. performed and analyzed electrophysiology experiments; A.H.S. performed and analyzed morphological analyses of iPSC-derived neurons; P.S. wrote analysis software and performed data analysis; C.T. wrote analysis software; E.G. developed and optimized analysis protocols; A.G. prepared autaptic cultures; M.P. and O.B. supervised human iPSC experiments; J.S.R. supervised autaptic culture experiments; J.S.R., N.B., A.H.S., E.G., K.R., M.P., and O.B. wrote the paper. All authors contributed to the final editing of the paper.

DECLARATION OF INTERESTS

O.B. is cofounder of and has stock in LIFE & BRAIN GmbH.

Received: October 11, 2018

Revised: February 5, 2019

Accepted: April 10, 2019

Published: May 14, 2019

REFERENCES

- Bardy, C., van den Hurk, M., Eames, T., Marchand, C., Hernandez, R.V., Kellogg, M., Gorris, M., Galet, B., Palomares, V., Brown, J., et al. (2015). Neuronal medium that supports basic synaptic functions and activity of human neurons *in vitro*. *Proc. Natl. Acad. Sci. USA* *112*, E2725–E2734.
- Bardy, C., van den Hurk, M., Kakaradov, B., Erwin, J.A., Jaeger, B.N., Hernandez, R.V., Eames, T., Paucar, A.A., Gorris, M., Marchand, C., et al. (2016). Predicting the functional states of human iPSC-derived neurons with single-cell RNA-seq and electrophysiology. *Mol. Psychiatry* *21*, 1573–1588.
- Beers, J., Gulbranson, D.R., George, N., Siniscalchi, L.I., Jones, J., Thomson, J.A., and Chen, G. (2012). Passaging and colony expansion of human pluripotent stem cells by enzyme-free dissociation in chemically defined culture conditions. *Nat. Protoc.* *7*, 2029–2040.
- Bekkers, J.M., and Stevens, C.F. (1991). Excitatory and inhibitory autaptic currents in isolated hippocampal neurons maintained in cell culture. *Proc. Natl. Acad. Sci. USA* *88*, 7834–7838.
- Blanpain, C., Daley, G.Q., Hochedlinger, K., Passegué, E., Rossant, J., and Yamanaka, S. (2012). Stem cells assessed. *Nat. Rev. Mol. Cell Biol.* *13*, 471–476.
- Burgalossi, A., Jung, S., Man, K.N., Nair, R., Jockusch, W.J., Wojcik, S.M., Brose, N., and Rhee, J.S. (2012). Analysis of neurotransmitter release mechanisms by photolysis of caged Ca²⁺ in an autaptic neuron culture system. *Nat. Protoc.* *7*, 1351–1365.
- Deshpande, A., Yadav, S., Dao, D.Q., Wu, Z.Y., Hokanson, K.C., Cahill, M.K., Wiita, A.P., Jan, Y.N., Ullian, E.M., and Weiss, L.A. (2017). Cellular Phenotypes in Human iPSC-Derived Neurons from a Genetic Model of Autism Spectrum Disorder. *Cell Rep.* *21*, 2678–2687.
- Dolmetsch, R., and Geschwind, D.H. (2011). The human brain in a dish: the promise of iPSC-derived neurons. *Cell* *145*, 831–834.
- Doudna, J.A., and Charpentier, E. (2014). Genome editing. The new frontier of genome engineering with CRISPR-Cas9. *Science* *346*, 1258096.
- Dovey, H.F., John, V., Anderson, J.P., Chen, L.Z., de Saint Andrieu, P., Fang, L.Y., Freedman, S.B., Folmer, B., Goldbach, E., Holsztynska, E.J., et al. (2001). Functional gamma-secretase inhibitors reduce beta-amyloid peptide levels in brain. *J. Neurochem.* *76*, 173–181.
- Hanna, J.H., Saha, K., and Jaenisch, R. (2010). Pluripotency and cellular reprogramming: facts, hypotheses, unresolved issues. *Cell* *143*, 508–525.
- Johnson, M.A., Weick, J.P., Pearce, R.A., and Zhang, S.C. (2007). Functional neural development from human embryonic stem cells: accelerated synaptic activity via astrocyte coculture. *J. Neurosci.* *27*, 3069–3077.
- Jucker, M. (2010). The benefits and limitations of animal models for translational research in neurodegenerative diseases. *Nat. Med.* *16*, 1210–1214.
- Klenke, C., Widera, D., Engelen, T., Müller, J., Noll, T., Niehaus, K., Schmitz, M.L., Kaltschmidt, B., and Kaltschmidt, C. (2013). Hsc70 is a novel interactor of NF-kappaB p65 in living hippocampal neurons. *PLoS ONE* *8*, e65280.
- Kotoglou, P., Kalaitzakis, A., Vezyraki, P., Tzavaras, T., Michalis, L.K., Dantzer, F., Jung, J.U., and Angelidis, C. (2009). Hsp70 translocates to the nuclei and nucleoli, binds to XRCC1 and PARP-1, and protects HeLa cells from single-strand DNA breaks. *Cell Stress Chaperones* *14*, 391–406.
- Lipstein, N., Verhoeven-Duif, N.M., Michelassi, F.E., Calloway, N., van Hasselt, P.M., Pienkowska, K., van Haaften, G., van Haelst, M.M., van Empelen, R., Cuppen, I., et al. (2017). Synaptic UNC13A protein variant causes increased neurotransmission and dyskinetic movement disorder. *J. Clin. Invest.* *127*, 1005–1018.
- Meijer, M., Rehbach, K., Brunner, J.W., Classen, J.A., Lammertse, H.C.A., van Linge, L.A., Schut, D., Krutenko, T., Hebisch, M., Cornelisse, L.N., et al. (2019). A single-cell model for synaptic transmission and plasticity in human iPSC-derived neurons. *Cell Rep.* *27*, this issue, 2199–2211.
- Nair, R., Lauks, J., Jung, S., Cooke, N.E., de Wit, H., Brose, N., Kilimann, M.W., Verhage, M., and Rhee, J. (2013). Neurobeachin regulates neurotransmitter receptor trafficking to synapses. *J. Cell Biol.* *200*, 61–80.
- Neher, E. (2015). Merits and Limitations of Vesicle Pool Models in View of Heterogeneous Population of Synaptic Vesicles. *Neuron* *87*, 1131–1142.
- Okita, K., and Yamanaka, S. (2011). Induced pluripotent stem cells: opportunities and challenges. *Philos. Trans. R. Soc. Lond. B Biol. Sci.* *366*, 2198–2207.
- Okuno, H. (2011). Regulation and function of immediate-early genes in the brain: beyond neuronal activity markers. *Neurosci. Res.* *69*, 175–186.
- Osafune, K., Caron, L., Borowiak, M., Martinez, R.J., Fitz-Gerald, C.S., Sato, Y., Cowan, C.A., Chien, K.R., and Melton, D.A. (2008). Marked differences in differentiation propensity among human embryonic stem cell lines. *Nat. Biotechnol.* *26*, 313–315.
- Pyott, S.J., and Rosenmund, C. (2002). The effects of temperature on vesicular supply and release in autaptic cultures of rat and mouse hippocampal neurons. *J. Physiol.* *539*, 523–535.
- Qian, K., Huang, C.T.-L., Chen, H., Blackbourn, L.W., 4th, Chen, Y., Cao, J., Yao, L., Sauvey, C., Du, Z., and Zhang, S.C. (2014). A simple and efficient system for regulating gene expression in human pluripotent stem cells and derivatives. *Stem Cells* *32*, 1230–1238.
- Regehr, W.G. (2012). Short-term presynaptic plasticity. *Cold Spring Harb. Perspect. Biol.* *4*, a005702.
- Rhee, J.S., Betz, A., Pyott, S., Reim, K., Varoqueaux, F., Augustin, I., Hesse, D., Südhof, T.C., Takahashi, M., Rosenmund, C., and Brose, N. (2002). Beta phorbol ester- and diacylglycerol-induced augmentation of transmitter release is mediated by Munc13s and not by PKCs. *Cell* *108*, 121–133.
- Ripamonti, S., Ambrozkiwicz, M.C., Guzzi, F., Gravati, M., Biella, G., Bor-muth, I., Hammer, M., Tuffy, L.P., Sigler, A., Kawabe, H., et al. (2017). Transient oxytocin signaling primes the development and function of excitatory hippocampal neurons. *eLife* *6*, e22466.
- Schotten, S., Meijer, M., Walter, A.M., Huson, V., Mamer, L., Kalogreades, L., ter Veer, M., Ruiter, M., Brose, N., Rosenmund, C., et al. (2015). Additive effects on the energy barrier for synaptic vesicle fusion cause supralinear effects on the vesicle fusion rate. *eLife* *4*, e05531.
- Shi, Y., Kirwan, P., and Livesey, F.J. (2012a). Directed differentiation of human pluripotent stem cells to cerebral cortex neurons and neural networks. *Nat. Protoc.* *7*, 1836–1846.
- Shi, Y., Kirwan, P., Smith, J., Robinson, H.P., and Livesey, F.J. (2012b). Human cerebral cortex development from pluripotent stem cells to functional excitatory synapses. *Nat. Neurosci.* *15*, 477–486.
- Sholl, D.A. (1953). Dendritic organization in the neurons of the visual and motor cortices of the cat. *J. Anat.* *87*, 387–406.
- Spanpanato, J., Sullivan, R.K., Turpin, F.R., Bartlett, P.F., and Sah, P. (2012). Properties of doublecortin expressing neurons in the adult mouse dentate gyrus. *PLoS ONE* *7*, e41029.

- Takahashi, K., and Yamanaka, S. (2016). A decade of transcription factor-mediated reprogramming to pluripotency. *Nat. Rev. Mol. Cell Biol.* *17*, 183–193.
- Tang, H., Sha, H., Sun, H., Wu, X., Xie, L., Wang, P., Xu, C., Larsen, C., Zhang, H.L., Gong, Y., et al. (2013). Tracking induced pluripotent stem cells-derived neural stem cells in the central nervous system of rats and monkeys. *Cell. Reprogram.* *15*, 435–442.
- Volpato, V., Smith, J., Sandor, C., Ried, J.S., Baud, A., Handel, A., Newey, S.E., Wessely, F., Attar, M., Whiteley, E., et al. (2018). Reproducibility of Molecular Phenotypes after Long-Term Differentiation to Human iPSC-Derived Neurons: A Multi-Site Omics Study. *Stem Cell Reports* *11*, 897–911.
- Weick, J.P., Johnson, M.A., Skroch, S.P., Williams, J.C., Deisseroth, K., and Zhang, S.C. (2010). Functional control of transplantable human ESC-derived neurons via optogenetic targeting. *Stem Cells* *28*, 2008–2016.
- Wierda, K.D., Toonen, R.F., de Wit, H., Brussaard, A.B., and Verhage, M. (2007). Interdependence of PKC-dependent and PKC-independent pathways for presynaptic plasticity. *Neuron* *54*, 275–290.
- Wojcik, S.M., and Brose, N. (2007). Regulation of membrane fusion in synaptic excitation-secretion coupling: speed and accuracy matter. *Neuron* *55*, 11–24.
- Wu, H., Xu, J., Pang, Z.P., Ge, W., Kim, K.J., Bianchi, B., Chen, C., Südhof, T.C., and Sun, Y.E. (2007). Integrative genomic and functional analyses reveal neuronal subtype differentiation bias in human embryonic stem cell lines. *Proc. Natl. Acad. Sci. USA* *104*, 13821–13826.
- Yang, N., Ng, Y.H., Pang, Z.P., Südhof, T.C., and Wernig, M. (2011). Induced neuronal cells: how to make and define a neuron. *Cell Stem Cell* *9*, 517–525.
- Yang, N., Chanda, S., Marro, S., Ng, Y.H., Janas, J.A., Haag, D., Ang, C.E., Tang, Y., Flores, Q., Mall, M., et al. (2017). Generation of pure GABAergic neurons by transcription factor programming. *Nat. Methods* *14*, 621–628.
- Zhang, Y., Pak, C., Han, Y., Ahlenius, H., Zhang, Z., Chanda, S., Marro, S., Patzke, C., Acuna, C., Covy, J., et al. (2013). Rapid single-step induction of functional neurons from human pluripotent stem cells. *Neuron* *78*, 785–798.

STAR★METHODS

KEY RESOURCES TABLE

REAGENT or RESOURCE	SOURCE	IDENTIFIER
Antibodies		
Mouse Ankyrin G	NeuroMab	Cat#75-146; RRID: AB_10673030
Mouse Ankyrin G (H-4)	SantaCruz Biotech.	Cat#sc-166602; RRID: AB_2057712
Rabbit C-Fos	SantaCruz Biotech.	Cat#sc-52; RRID: AB_2106783
Rabbit doublecortin	Abcam	Cat#ab18723; RRID: AB_732011
Mouse Gephyrin 3B11	Synaptic Systems	Cat#147111; RRID: AB_887719
Guinea Pig GFAP	Synaptic Systems	Cat#173004; RRID: AB_10641162
Mouse HSC 70 (B-6)	Santa Cruz Biotech.	Cat#sc-7298; RRID: AB_627761
Chicken MAP2	Novus Biologicals	Cat# NB300-213; RRID: AB_350528
Guinea Pig Shank2	Synaptic systems	Cat#162 204; RRID: AB_2619861
Mouse SMI-312	HISS Diagnostics	Cat#SMI-312R; RRID: AB_2619861
Rabbit VGAT	Synaptic Systems	Cat#131011; RRID: AB_887872
Mouse VGAT	Synaptic Systems	Cat#131002; RRID: AB_887871
Rabbit VGluT1	Synaptic Systems	Cat#135511; RRID: AB_887879
Rabbit VGluT1	Synaptic Systems	Cat#135302; RRID: AB_887877
Mouse BRN2	Santa Cruz	Cat#SC393324; RRID: AB_2737347
Mouse Calbindin	Swant	Cat#300; RRID: AB_10000347
Mouse Calretinin	Swant	Cat#6B3; RRID: AB_00003201
Rat CTIP2	Abcam	Cat#18465; RRID: AB_2064130
Rabbit DLX2	ThermoFisher	Cat#702009; RRID: AB_2723069
Mouse Human Nuclei	Millipore	Cat#MAB4383; RRID: AB_827439
Rabbit GABA	Sigma	Cat#A-2052; RRID: AB_477652
Rabbit FOXP1	Abcam	Cat#18259; RRID: AB_732415
Rabbit Parvalbumin	ThermoFisher	Cat#PA1-933; RRID: AB_2713898
Mouse SST	R&D Systems	Cat#MAB2358; RRID: AB_2722572
Mouse TBR1	Proteintech	Cat#209321AP; RRID: AB_10695502
Rabbit TUJ1	Biolegend	Cat#802001; RRID: AB_2564645
Mouse TUJ1	Biolegend	Cat# 801202; RRID: AB_10063408
Alexa Fluor 405 Goat anti-Chicken	abcam	Cat#ab175674
Alexa Fluor 488 Goat anti-Guinea Pig	Life	Cat#A11073; RRID: AB_142018
Alexa Fluor 488 Goat anti-Mouse	Thermo Fisher	Cat#A11001; RRID: AB_2534069
Alexa Fluor 488 Goat anti-Rabbit	Thermo Fisher	Cat#A11008; RRID: AB_143165
Alexa Fluor 488 Goat anti-Mouse	Life	Cat#A11029; RRID: AB_2534088
Alexa Fluor 488 Goat anti-Chicken	Thermo Fisher	Cat#A11039; RRID: AB_2534096
Alexa Fluor 555 Goat anti-Rat	Thermo Fisher	Cat#A11006; RRID: AB_2534074
Alexa Fluor 555 Goat anti-Mouse	Thermo Fisher	Cat#A21429; RRID: AB_2535850
Alexa Fluor 555 Goat anti-Rabbit	Thermo Fisher	Cat#A21424; RRID: AB_141780
Alexa-555-labeled streptavidin	Thermo Fisher	Cat#S32355; RRID: AB_2307336
Alexa Fluor 568 Goat anti-Mouse	abcam	Cat#ab175714
Alexa Fluor 568 Goat anti-Rabbit	Thermo Fisher	Cat#A11011; RRID: AB_143157
Alexa Fluor 633 Goat anti-Guinea Pig	Thermo Fisher	Cat#A21105; RRID: AB_2535757
Alexa Fluor 633 Goat anti-Mouse	Thermo Fisher	Cat#A21052; RRID: AB_2535719
Alexa Fluor 633 Goat anti-Rabbit	Thermo Fisher	Cat#A21071; RRID: AB_2535732

(Continued on next page)

Continued		
REAGENT or RESOURCE	SOURCE	IDENTIFIER
Bacterial and Virus Strains		
One Shot TOP10 chemically competent e. coli	Thermo Fisher	Cat#C404010
Chemicals, Peptides, and Recombinant Proteins		
Bicuculline	Tocris	Cat#0130 CAS 40709-69-1
Biocytin	Sigma	Cat#B4261 CAS 576-19-2
EGF recombinant human protein	ThermoFisher Scientific	Cat#PHG0311
Mito Serum Extender	Corning	Cat#355006
NBQX	HelloBio	Cat#HB0443 CAS 479347-86-9
Phorbol-12,13-dibutyrate (PDBu)	Calbiochem	Cat#524390 CAS 37558-16-0
Tetrodotoxin (TTX)	Tocris	Cat#1078 CAS 18660-81-6
Recombinant human BDNF	Peprotech	Cat#450-02
Recombinant human BDNF	Cell GS	Cat#GFH1
Recombinant human GDNF	Peprotech	Cat#450-10
Dibutyryl cAMP	Sigma	Cat#D0260
Accutase	GIBCO	Cat#A11105-01
AraC	Sigma	Cat#C1768
DAPT	Sigma	Cat#D5942-5MG
Doxycycline	Sigma	Cat#D9891-1G,
EDTA	Sigma	Cat#E6635
Laminin	Sigma	Cat#L2020
LDN193189	Axon Medchem	Cat#Axon1509
Y-27632 (ROCK-inhibitor)	Tocris	Cat#1254 CAS 129830-38-2
Y-27632 (ROCK inhibitor)	Cellagen Technology LLC	Cat#C9127-2
SB431542	Axon Medchem	Cat#13031-25
Experimental Models: Cell Lines		
C-62 m-s3 iPSCs (generation of GlutNs x 3)	Rehbach et al., in revision	N/A
C-62 m-s4 iPSCs (generation of GlutNs x 2)	Rehbach et al., in revision	N/A
C-62 m-s4 iPSCs (generation of GABANs x 3)	Rehbach et al., in revision	N/A
C-61f-s2 iPSCs (generation of GABANs x 3)	Rehbach et al., in revision	N/A
C-14 m-s11 NGN2 iPSCs (generation of iGlutNs x 5)	Generated in this study	N/A
C-35 m-r1 NGN2 iPSCs (generation of iGlutNs x 3)	Generated in this study	N/A
C-133bm-s4 ADP#8 iPSCs (generation of iGABANs x 2)	Generated in this study	N/A
Experimental Models: Organisms/Strains		
Mouse: C57BL/6N	The Jackson Laboratory	MGI Cat# 5701513, RRID:MGI:5701513
Rat: Wistar	Charles River	RRID: RGD_10395228MGI
Oligonucleotides		
Fwd primer: ACCAACGCCGACGGTATCAG	Integrated DNA Technologies	N/A
Rv1 primer: CAGACCCTTGCCCTGGTGGT	Integrated DNA Technologies	N/A
Rv2 primer: CACCAGGATCAGTGAAACGC	Integrated DNA Technologies	N/A
Recombinant DNA		
AAVS1-GFP	Dr. Su-Chun Zhang (University of Wisconsin) (Qian et al., 2014)	https://doi.org/10.1002/stem.1653
AAVS1-NGN2	Meijer et al., this issue	N/A
AAVS1-APD	Generated in this study	N/A
AAVS1-TALEN-L	Dr. Su-Chun Zhang (University of Wisconsin) (Qian et al., 2014)	https://doi.org/10.1002/stem.1653
AAVS1-TALEN-R	Dr. Su-Chun Zhang (University of Wisconsin) (Qian et al., 2014)	https://doi.org/10.1002/stem.1653

(Continued on next page)

Continued

REAGENT or RESOURCE	SOURCE	IDENTIFIER
Software and Algorithms		
AxoGraph (Version 1.5.4)	Axograph Scientific	https://axograph.com/download/axograph
Clampex program (Ver. 10.1)	Molecular Devices	http://mdc.custhelp.com/app/answers/detail/a_id/18779/~/axon%E2%84%A2pclamp%E2%84%A2-10-electrophysiology-data-acquisition-%26-analysis-software-download
GraphPad Prism (Version 5 and 7)	GraphPad Software Inc.	https://www.graphpad.com/
PatchMaster program (Version 2X90.3)	HEKA electronics	https://www.heka.com/downloads/downloads_main.html
ImageJ (Version 1.5i and 1.52d)	National Institutes of Health	https://imagej.nih.gov/ij/download/
SigmaPlot (Version 14)	Systat Software Incorporated	https://systatsoftware.com/downloads/
CorelDRAW (Version 19.1.0.419)	Corel Corporation	https://www.coreldraw.com/en/product/coreldraw/?topNav=en
Adobe Photoshop CC (Version 19.1.6)	Adobe Systems Incorporated	https://www.adobe.com/products/photoshop.html
INCell Analyzer 2200 software	GE Healthcare	https://www.gelifesciences.com/en/de/shop/cell-imaging-and-analysis/high-content-analysis-systems/instruments/in-cell-analyzer-2200-p-00558
INCell developer toolbox	GE Healthcare	https://www.gelifesciences.com/en/de/shop/cell-imaging-and-analysis/high-content-analysis-systems/instruments/in-cell-analyzer-2200-p-00558
GenomeStudio	Illumina	https://www.illumina.com/techniques/microarrays/array-data-analysis-experimental-design/genomestudio.html

CONTACT FOR REAGENT AND RESOURCE SHARING

Requests for resources, reagents, and further information should be directed to the Lead Contact, JeongSeop Rhee (rhee@em.mpg.de). Questions relating to cell generation can be directly addressed to Michael Peitz (peitz@uni-bonn.de). Protocols, information, and unique tools and reagents regarding autaptic cultures and their electrophysiological and morphological analysis can be obtained from JeongSeop Rhee (rhee@em.mpg.de).

EXPERIMENTAL MODEL AND SUBJECT DETAILS**iPSCs - source and generation**

The use of all iPSC lines was approved by the Ethics Committee of the Medical Faculty of the University of Bonn (approval 275/08), and informed written consent was obtained from the donors. All experiments were performed in accordance with German guidelines and regulations. The following numbers of cell lines and *in vitro* differentiations were performed: GlutNs, 5 sets of *in vitro* differentiations; GABANs, 2 lines, 3 sets of *in vitro* differentiations per line; iGlutNs, 2 lines, 5 and 3 sets of *in vitro* differentiations, respectively; iGABANs, 2 sets of *in vitro* differentiations.

Mouse maintenance

Animal experiments were done in compliance with applicable animal care guidelines and performed as approved (Lower Saxony State Office for Consumer Protection and Food Safety; permits 33.9-42502-04-13/1359 and 33.19-42502-04-15/1921). Animals were kept in groups according to European Union Directive 63/2010/EU and ETS 123 (individually ventilated cages, specific pathogen-free conditions, 21 ± 1°C, 55% relative humidity, 12 h/12 h light/dark cycle). Mice received food and tap water *ad libitum* and were provided with bedding and nesting material. Cages were changed once a week. Animal health was controlled daily by caretakers and by a veterinarian. Health monitoring (serological analyses; microbiological, parasitological, and pathological examinations) was done quarterly according to FELASA recommendations with either NMRI sentinel mice or animals from the colony. The mouse colony used for experiments did not show signs of pathogens. The sex of animals used for experimentation was not checked because all previous studies had indicated that the sex does not affect the parameters studied here.

METHOD DETAILS

Differentiation of iPSCs into glutamatergic cortical neurons

iPSCs were cultured in mTeSR (StemCell Technologies) or StemMACS iPS-Brew (Miltenyi Biotec) and split with EDTA during maintenance (Beers et al., 2012). Undifferentiated iPSCs were seeded as single cells at high density (1×10^6 cells per cm^2) in iPSC medium with 10 μM ROCK inhibitor (RI) Y-27632 (Tocris). The next day, the medium was switched to GLUT neural induction medium (3N medium with 1 μM Dorsomorphin/200 nM LDN-193189, 10 μM SB431542). 3N medium consists of 49% DMEM/F12, 49% Neurobasal medium, 1% B27 supplement, 0.5% NEAA, 0.5 mM GlutaMax, 50 μM β -mercaptoethanol, 10 nM progesterone, 50 μM putrescine, 30 nM sodium selenite, 50 ng/ml apo-transferrin, 12.5 $\mu\text{g/ml}$ insulin, 0.8 mg/ml glucose (ThermoFisher Scientific or Sigma). On day 11, the medium was switched to 3N with 20 ng/ml FGF2 to promote neural rosette formation. On day 12, cultures were split using accutase (ThermoFisher Scientific). Obtained cells were propagated in 3N medium with 20 ng/ml FGF2 and 10 μM RI at a split ratio of 1:3 in Matrigel (MG)-coated (Corning) 6-well plates. Starting on day 14, FGF2 was reduced to 10 ng/ml and 100 ng/ml heparin was added. On day 18 and day 22, cultures were dissociated as clumps and seeded at a split ratio of 1:2 on fresh MG-coated plates for further propagation. On day 32, cortical progenitors were dissociated with accutase in the presence of 10 μM RI for 20 minutes at 37°C and frozen down as one batch in ice-cold freezing medium (90% KOSR, 10% DMSO). For further maturation after thawing, cryopreserved progenitors were seeded in 3N medium supplemented with 10 μM RI on MG-coated plates (0.5×10^6 cells per cm^2). On day 44, cultures contained a large fraction of neurons and were dissociated and seeded for final maturation. On the next day, the medium was changed to 3N medium with 10 ng/ml BDNF, 10 μM PD0325901, and 10 μM DAPT to promote differentiation of remaining precursors. The same medium was refreshed on day 47. On day 49, the cultures were mitotically inactivated by 5 μM AraC (cytosine β -D-arabinofuranoside hydrochloride), to prevent further proliferation, and treated with 10 ng/ml BDNF. On day 50, AraC-containing medium was removed carefully and replaced by 3N with 10 ng/ml BDNF. On day 51, neurons were frozen as a large batch as described below.

Differentiation of iPSCs into GABAergic forebrain neurons

To generate GABAergic forebrain differentiation, iPSCs were cultured in E8 medium and split with EDTA during maintenance (Beers et al., 2012). Undifferentiated iPSCs were seeded as single cells at a density of 0.2×10^6 per cm^2 in E8 medium supplemented with 10 μM RI. The next day, the medium was switched to GABA neural induction medium (N2/B27, 500 nM LDN-193189, 15 μM SB431542). N2/B27 consists of 49% DMEM/F12, 0.5% N2 supplement, 49% neurobasal medium, 1% B27 supplement, 0.5% NEAA, 0.5 mM L-glutamine, 50 μM β -mercaptoethanol. On day 9, the neural induction medium was supplemented with 20 ng/ml FGF2 to promote neural rosette formation. On day 10, the cultures were split using accutase. Obtained cell clumps were seeded in N2/B27 medium with 20 ng/ml FGF2 and 10 μM RI at a split ratio of 1:3 onto MG-coated 6-well plates. The cultures were cultivated in N2/B27 medium supplemented with 20 ng/ml FGF2 until day 12. Cells were further propagated in N2/B27 medium which was changed every other day. On day 20, progenitors were dissociated and frozen as one batch in ice-cold freezing medium. For maturation of cryopreserved progenitors, cells were seeded in N2/B27 medium with 10 μM RI (0.5×10^6 cells per cm^2). On day 25, cultures were mitotically inactivated with 5 μM AraC to prevent further proliferation and carefully removed after 24 h. On day 27, neurons were frozen as a large batch.

Plasmid cloning for forward programming

AAVS1-GFP plasmid and the corresponding TALEN pair were provided by Dr. Su-Chun Zhang (University of Wisconsin) (Qian et al., 2014). To establish the AAVS1-ASCL1-P2A-DLX2 (AAVS1-APD) targeting construct, the GFP coding sequence was removed from the AAVS1-GFP plasmid and replaced with an ASCL1-P2A-DLX2 cassette, which was designed *in silico* based on codon-optimized human coding sequences and synthesized (GeneArt). After cutting from the cloning plasmid, the cassette was inserted into the AAVS1-backbone via conventional ligation.

iPSC nucleofection for AAVS1 targeting

AAVS1-targeted iPSC lines were generated by nucleofecting 3–4 million cells with the corresponding targeting plasmid (4 μg) together with the TALEN pair (0.5 μg each) using the Amaxa nucleofection kit V (Lonza) with program B-023 after a preincubation step with 10 μM of RI for 1 h. Nucleofected iPSCs were seeded on Geltrex-coated dishes (ThermoFisher Scientific) at low density in StemMACS iPS Brew (Miltenyi Biotec) with 10 μM RI as well as 5 μM L755507. After 24 h, medium was replaced with StemMACS iPS Brew including 10 μM RI, and renewed every other day. RI was supplemented until the formation of small puromycin-resistant colonies and then discontinued. Puromycin selection (0.3 $\mu\text{g/ml}$) was started at 48 h post-nucleofection and maintained for at least 7 days. Resistant colonies were picked, expanded, and analyzed via genotyping PCR. Site-specific transgene insertion was validated by PCR using the following primer combination: fwd, ACCAACGCGGACGGTATCAG; rv1, CAGACCCTTGCCCTGGTGGT; rv2, CACCAGGATCAGTAAAACGC.

Forward programming of iPSCs into GABAergic forebrain neurons

Before the start of differentiation, iPSCs were maintained in StemMACS iPS-Brew (Miltenyi Biotec) and split with EDTA 2–3 times. To start differentiation, iPSCs were seeded as single cell suspension in Geltrex-coated six-well plates at a density of 40,000 cells/ cm^2

and maintained in iPSC medium. Two days later, the medium was switched to N2 neural induction medium containing 2 $\mu\text{g}/\text{ml}$ doxycycline. On day 2 after induction, cells were dissociated with accutase and plated in laminin-coated T175 flasks at a density of 100,000 cells/ cm^2 in NB/B27 medium containing doxycycline. On day 3 after induction, 10 μM DAPT was added and kept until day 6. The cells were treated with 5 μM AraC on day 7 and cryopreserved as a large batch on day 9 as described below. Details of the generation of iGlutNs by expression of NGN2 are provided in the accompanying paper (Meijer et al., 2019).

Cryopreservation of post-mitotic neurons

Two days after AraC treatment, neurons were cryopreserved as a single batch. Neuronal cultures were dissociated slowly by incubating accutase supplemented with 10 μM RI for 60–90 min at 37°C. Cells were washed off with warm medium, dissociated further by pipetting, and passed through a cell strainer. The cell solution was divided into several falcon tubes, and centrifuged at 300 \times g for 5 min. Subsequently, the cells were resuspended in ice-cold freezing medium (70% KOSR, 20% 1 M trehalose, 10% DMSO) and deep frozen with a rate of approximately $-1^\circ\text{C}/\text{min}$. Cells remaining in the cell strainer were collected for DNA analysis.

Immunostaining of immature neuronal batches

For QC, neurons were thawed, counted, and seeded on 96-well plates (ibidi, μ -plates) in NB/B27 medium supplemented with 10 μM RI. After 7 days, neurons were fixed with freshly thawed pre-warmed 4% PFA for 10–15 min. For the fixation of GABA, the PFA solution was supplemented with 0.04% glutaraldehyde. Cultures were blocked with 10% FBS in PBS + 0.1% Triton X-100 for one hour. The primary antibodies were diluted in 10% FBS in PBS + 0.1% Triton X-100 and incubated over night at 4°C. Afterward, adequate secondary antibodies were diluted in 10% FBS in PBS + 0.1% Triton X-100 and incubated for one hour. The following antibodies were used: BRN2 (ms IgG, Santa Cruz, sc-393324, 1:500; rb IgG, Abcam 94977, 1:500), CTIP2 (rat IgG, Abcam, ab18465, 1:500), GABA (ms IgG, Sigma, A0310, 1:1000; rb IgG, Sigma, A2052), TBR1 (rb IgG, Proteintech, 20932-1-AP, 1:1000), TUJ1/ β 3-tubulin (ms IgG, Covance, MMS-435P, 1:1000; rb IgG, Covance, PRB-435P, 1:2000; ck IgY, Milipore, AB9354), VGluT1 (rb IgG, Synaptic Systems, 135303, 1:1000), VGluT2 (rb IgG, Abcam ab84103), FOXG1 (rb IgG, Abcam, ab18259). Images were acquired using the InCell analyzer 2000 (GE Healthcare). Cellular markers were quantified automatically using the InCell Developer toolbox.

Preparation of astrocyte micro-island cultures

Astrocyte micro-island plates were prepared and cultured as previously reported (Burgalossi et al., 2012). Briefly, a human astrocyte cell line (ScienCell) was cultured and maintained until use in complete astrocyte medium (ScienCell) with 0.1% penicillin/streptomycin or DMEM (with GlutaMax, GIBCO), 1% N2 supplement, 10% FBS (GIBCO) and 20 ng/ml EGF recombinant human protein (ThermoFisher Scientific). Mouse and rat astrocytes for autaptic cultures were obtained from mouse and rat cortices dissected from P0 wild-type animals and enzymatically digested for 15 min at 37°C with 0.05% (w/v) trypsin-EDTA. Astrocytes were plated in T75 culture flasks in DMEM (containing 10% FBS, 20 U/ml penicillin, 20 $\mu\text{g}/\text{ml}$ streptomycin, Mito Serum Extender (Corning)) and grown for 7–10 days *in vitro* (DIV). The different astrocyte species were trypsinized and plated at a density of 30,000 cells/well onto 32 mm^2 -diameter glass coverslips that had previously been coated with agarose (Sigma) and stamped using a custom-made stamp to generate 400 μm \times 400 μm substrate islands with a coating solution containing poly-D-lysine (Sigma), acetic acid, and collagen (BD Biosciences).

Mouse forebrain cortical neuron culture

P0 mouse forebrains were isolated and digested for 80 min at 37°C in DMEM containing 25 U/ml papain (Worthington Biomedical Corporation), 0.2 mg/ml cysteine (Sigma), 1 mM CaCl_2 , and 0.5 mM EDTA. After washing, the dissociated cortical neurons were seeded onto the micro-island plates in pre-warmed Neurobasal medium supplemented with B27, Glutamax, and penicillin (100 U/ml)/streptomycin (100 $\mu\text{g}/\text{ml}$) at a density of 4,000 cells/well of 6-well plates. The neurons were allowed to mature for 10–12 days before electrophysiological assays.

Recovery and culture of cryopreserved human iPSC-derived neurons

One ml of cryopreserved neurons were quickly thawed in a 37°C water bath and diluted into 9 mL of pre-warmed N3 medium. After passing through a 40 μm cell strainer (BD Falcon) into 50 mL tubes, viable cells were counted using Trypan Blue staining. Different numbers of cells (GlutNs, 3,000; iGlutNs, 80,000; GABANs, 3,000, iGABANs, 6,000 cells/well of 6-well plates) were plated onto the astrocyte micro-island plates with 2 mL of N3 medium supplemented with 5 μM RI (Tocris). Cells were placed into the 37°C incubator for 24 h. On the next day, the whole medium was changed with 2 mL of different conditioned fresh N3 medium without ROCK inhibitor, depending on the culture. Medium was changed continuously once per week until cells were used. N3 medium consists of 49% DMEM/F12, 49% Neurobasal medium, 1% B27 supplement, 1% N2 supplement, 50 μM β -mercaptoethanol, 1 mM L-Glutamine, 0.5% NEAA with or without 0.5% FBS or 2 $\mu\text{g}/\text{ml}$ Doxycycline (Sigma). BrainPhys Neuronal medium (STEMCELL) consists of NeuroCult SM1, Neuronal Supplement (STEMCELL technologies), N2 Supplement-A (STEMCELL technologies), recombinant human BDNF (Peprotech), recombinant human GDNF (Peprotech), dibutyl cAMP (Sigma), and L-Ascorbic Acid (Sigma). All materials for cell cultures were purchased from Life Technology unless mentioned otherwise.

Immunofluorescence staining and imaging

Human neurons were fixed with 4% paraformaldehyde in PBS, pH 7.4, for 20 min at room temperature and then washed with PBS, quenched with 50 mM Glycine for 10 min and washed with PBS. Samples were incubated with iT-FX image enhancer (Life Technologies) in PBS for 20 min. The permeabilization steps were performed either with 0.1, 0.2, or 0.3% Triton X-100 and 2.5% normal goat serum (NGS) in PBS for 30 or 45 min at room temperature. The neurons were then incubated with the primary antibodies for 1 h. After washing with 0.1% Triton X-100/2.5%NGS/PBS, they were incubated with the secondary antibodies for 45 min, followed by extensive washing steps with 0.1% Triton X-100/2.5%NGS/PBS and PBS. The samples were then mounted with Aqua-Poly Mount mounting medium. Confocal acquisition of images was done with Leica SP2 and SP5 microscopes, with 40X, 60X, or 100X objectives with numerical apertures of 1.25, 1.4, and 1.45, respectively. Ar 65 mW 488 nm, HeNe 1 mW 633 nm, and DPSS 20 mW 561 nm lasers were used. White light laser (WLL, 1.5 mW) with a range from 470 to 670 nm with 70% power was used when fluorescence intensity needed to be quantified. The generated images were analyzed by Fiji and ImageJ (NIH). Synapse counting was done by in-house written IJ1 macros that isolate presynaptic structures, apply thresholds, convert to a mask, and then create a selection that is multiplied by 1 pixel size. The same steps were repeated for postsynaptic structures without the selection enlargement step, and colocalizing punctae were counted as synapses. Sholl analysis was made as described (Ripamonti et al., 2017; Sholl, 1953). For quantifying fluorescence intensities, the data were acquired for all the different conditions of a given set of experiments at the same day. Background was subtracted and intensities at the cell bodies were quantified by drawing a selection and measuring the mean gray value. For quantification of intensities at the neurites, segmented line scans of thickness three were used. Graphs and analysis were mainly generated with GraphPad Prism versions 5 and 7 and in some cases with SigmaPlot 13.

Electrophysiology

For whole-cell voltage-clamp recordings, cells were held at -70 mV, and holding voltage was increased to 0 mV (2 ms) to depolarize cells (MultiClamp 700B amplifier, Axon Instruments, Molecular Devices) under the control of the Clampex program 10.1 (Molecular Devices). The flow of extracellular solution was maintained during recordings and pharmacological solutions were applied if required. Hypertonic sucrose solution (0.5 M in external solution) was used to trigger fusion of the readily releasable pool of vesicles (RRP). NBQX (HelloBio) and Bicuculline (Tocris) were used to inhibit AMPA and GABA receptors, respectively. Miniature PSCs were recorded in the presence of 300 nM TTX (Tocris). The extracellular solution contained 140 mM NaCl, 2.4 mM KCl, 10 mM HEPES, 10 mM Glucose, 4 mM CaCl_2 , 4 mM MgCl_2 (320 mOsmol/liter), and the patch-pipette solution for recording contained 136 mM KCl, 17.8 mM HEPES, 1 mM EGTA, 4.6 mM MgCl_2 , 4 mM NaATP, 0.3 mM Na_2GTP , 15 mM creatine phosphate, and 5 U/ml phosphocreatine kinase (315 – 320 mOsmol/liter), pH 7.4. Cells were visualized by an inverted microscope (Olympus or Zeiss). Custom-made manipulators controlled the movement of the microelectrode. All drugs were applied with a custom-built fast flow system consisting of an array of flow pipes controlled by a stepper motor that allows complete and rapid solution exchange with time constants of ~ 30 ms. Pressure was on for 20 ms. Measurements were performed and registered using an Axon 700B Amplifier (Axon Instruments) and signals were converted with an Axon Instrument digitizer. Recording rate was 10 kHz. Microelectrodes were made by using a Sutter 2000 filament-based horizontal puller and used only if they had pipette resistances of 2.5 – 4.5 M Ω . Serial resistance was compensated by 35% – 60% and cells with serial resistances below 12 M Ω were analyzed. All chemicals were purchased from Sigma, unless mentioned otherwise. In the current clamp mode, whole-cell recordings were performed with a HEKA EPC-9USB amplifier and Patch-Master (Ver. 2X90.3) software (HEKA electronics). Measurements of R_{input} were calculated from membrane potential changes in response to subsequent 1 s current injections from -100 to 0 pA at 20 pA intervals. APs were generated by progressive incremental depolarizing current injection of $+5$ pA starting at 0 pA. All active electrical properties were analyzed in the first trace in which APs were evoked. The external solution for AP recording was the same as the solution used for analyses of synaptic currents (see above). The patch-pipette solution contained 138 mM K-gluconate, 16.8 mM HEPES, 10 mM NaCl, 1 mM $\text{MgCl}_2 \cdot 6\text{H}_2\text{O}$, 0.25 mM EGTA, 4 mM ATP- Mg^{2+} , 0.3 mM GTP- Na^+ (solution adjusted to pH 7.4, ~ 320 mOsmol/liter). Voltage gated sodium and potassium currents ($I_{\text{Na/K}}$) in neurons were evoked by 500 ms test pulses from a holding potential of -70 mV to set potentials between -80 mV and $+70$ mV (10 mV intervals). I_{K} was recorded with same protocol in the presence of 300 nM TTX. I_{Na} was obtained by subtracting the traces of I_{K} from the $I_{\text{Na/K}}$ traces. External and internal solutions were the same as for the current clamp recordings described above. Total outward K^+ currents (I_{K}) were evoked by 500 ms depolarizing test pulses from a holding potential of -70 mV to set potentials between -80 mV and $+70$ mV (10 mV intervals), and I_{DR} was measured with the same protocol in the presence of 1 mM 4AP. I_{A} traces were obtained by subtracting the I_{DR} from I_{K} . The external solution for the measurement of potassium currents contained 150 mM choline-Cl, 5 mM KCl, 1.5 mM CaCl_2 , 10 mM HEPES, 1 mM MgCl_2 , 0.2 mM CdCl_2 , 10 mM Glucose (solution adjusted to pH 7.3, ~ 310 mOsmol/liter). The internal solution contained 138 mM K-gluconate, 16.8 mM HEPES, 10 mM NaCl, 1 mM $\text{MgCl}_2 \cdot 6\text{H}_2\text{O}$, 0.25 mM EGTA, 4 mM ATP- Mg^{2+} , 0.3 mM GTP- Na^+ (solution adjusted to pH 7.4, ~ 320 mOsmol/liter). The densities of all voltage gated ion currents were normalized to cell membrane capacitance (pF). All electrophysiology data were analyzed using Axograph (Ver.1.5.4) software (Axograph Scientific).

QUANTIFICATION AND STATISTICAL ANALYSIS

Statistical analysis of data was performed with GraphPad Prism (Versions 5 or 7) software (GraphPad Software Inc.). Statistical comparisons between two groups of data were made using two-tailed unpaired Student's *t* test and Mann Whitney test. Multiple comparisons were determined using one-way analysis of variance (ANOVA) followed by post hoc testing (Tukey's, Dunn's and Kruskal-Wallis multiple comparison tests). *p-values* less than 0.05 were considered significant for single and multiple comparisons, respectively. Data are presented as mean \pm SEM.